SIMULATION OF PURE AND IMPURITY F-TYPE CENTERS IN NaF

by

Zhengguang Yang

A thesis

presented to the University of Manitoba

in partial fulfillment of the

requirements for the degree of

Master of Science

in

Physics

Winnipeg, Manitoba

ISBN 0-315-76954-8

SIMULATION OF PURE AND IMPURITY F-TYPE CENTERS IN NaF

BY

ZHENGGUANG YANG

A thesis submitted to the Faculty of Graduate Studies of the University of Manitoba in partial fulfillment of the requirements of the degree of

MASTER OF SCIENCE

Abstract

The recently found $(F_2^+)^*$ center, an F_2^+ center with divalent-impurity doping, has potential practical laser applications and also an unknown atomistic configuration. A simulation, based on unrestricted Hartree-Fock quantum-cluster calculations, is carried out to investigate the ground-state atomistic and electronic configurations of this center, and to test a proposed model for it. In order to avoid the complexity of this center, a simplified single-electron quantum-cluster model is employed, with effective shell-model short-range potentials derived from all-electron quantum-cluster calculations. For all configurations studied, an F-center like ground state is found. The interpretation of different configurations for this center is discussed with respect to stabilizing energies. Two configurations obtained are more favorable than the proposed model. In the present work, the F-center and the F_2^+-center ground states are also examined.

Acknowledgements

First of all, I would like to extend my deep gratitude to Professor John M. Vail for his continuous encouragement and guidance that made the present work possible. Secondly, I am very grateful to my wife, Xiaoyan, for her invaluable support and understanding throughout my study here in Canada. My sincere thanks also go to Professor John H. Page and Professor Barbara L. Sherriff for their time spent to examine this thesis and their helpful discussions. Finally, the assistance from the Department of Computer Service at the University of Manitoba is gratefully acknowledged.

Contents

List of Tables

List of Figures

Chapter 1

Introduction

With the help of highly-developed computational techniques and facilities nowadays, theoretical calculation of the electronic properties of point defects in ionic crystals has been making a great deal of progress in recent years, along with the experiments which are always essential to this field. Among those defects mostly studied, the F-type centers in alkali halides have attracted particular interest because of their roles in laser application. Ordinary F-type center lasers have poor stability and low quantum efficiency at room temperature, and therefore are mostly unsuitable for laser application. The recently found $(F_2^+)^*$ center, a divalent impurity-doped F_2^+ center, shows dramatically improved room temperature stability and higher quantum efficiency. The investigation of this center points to an imminent and promising future for producing a practical laser device.

A theoretical simulation of the $(F_2^+)^*$ center in the crystal lattice NaF has been carried out in this thesis to further investigate a model recently proposed for this center. It is hoped that the present work would either provide a better insight into the nature of the $(F_2^+)^*$ center, or set up a proper starting point for future research on it. Unlike ordinary F-type centers, which usually have symmetrical and fairly compact structures, the $(F_2^+)^*$ center has a more complicated structure with low symmetry, and is spread out over several atomic sites. Furthermore, experiments to date indicate that it is not yet clear what the true configuration is for

this center. Usually, point defect calculations in ionic crystals are based on the quantum-mechanical cluster treatment. However, for the $(F_2^+)^*$ center, this can be impractical, because investigating the proposed model requires considering a variety of different configurations, each one leading to very large quantum-cluster calculations. For computer simulation of this center, considerably simplified treatments are required. For this purpose, a model consisting of a single-electron quantum cluster with effective classical potentials is proposed in this simulation.

Chapter 2 gives a brief review of some F-type centers and their properties. Also, the laser effects and some applications of these centers are presented. We hope that this could serve two purposes. The first is to serve as an introduction for students who are new to the field of point defects in solids, especially F-type centers in ionic crystals. The second is to provide a fundamental background for the present work.

In chapter 3, a general model for electronic defect calculations without our simplifying consideration is introduced. This includes mainly two aspects: the Hartree-Fock self-consistent field method, and the shell model, for quantum-mechanical and classical treatments of crystals, respectively. In section 3.3, the computer program ICECAP and its methodology are briefly presented, combining a Hartree-Fock cluster and a shell-model lattice consistently.

Chapter 4 contains the major results of our research, including the simplified model we have used and all preliminary work needed for applying the model to the principal problem. First, the single-electron model for simulating the $(F_2^+)^*$ center is presented in section 4.1. Then in the next three sections, under the quantum-mechanical many-electron cluster treatment, we investigate the F and the F_2^+ centers, and derive the effective classical short-range potentials, using the mathematical and physical models described in chapter 3. Specifically, the Mg^{2+}-F^- potential is derived in section 4.2; the results of the F- and F_2^+-center ground states are presented and discussed in section 4.3; and in section 4.4, the short-range potentials

are derived for interactions between F-type centers and ions. In the last section of chapter 4, based on all the work in the previous sections, we apply the simplified single-electron model to the central problem, the $(F_2^+)^*$ center, analyzing a variety of possible configurations. The results are listed and discussed in some detail. The interpretation of different configurations in terms of stabilizing energies is also given in this section.

Finally, the conclusions of the present work are given, and proposals for future work are discussed in chapter 5.

Chapter 2

F-type Centers and Lasers

The phenomenon of coloration in alkali halide materials, which have the rock-salt structure, can be traced back to about a century ago. But only after Pohl and coworkers, in the thirties, first observed the coloration in KBr by heating the crystal at 600°C in potassium vapor [1], did it attract serious attention. Since then, the coloration in ionic crystals has been under extensive investigation. It was found to be due to the point defects, which were named color centers, or F centers (after a German word, Farben) by Pohl *et al* [1]. At first, the focus was mainly on the F center, but later other F-type centers were found. Seitz first proposed F-aggregate-center models [2] based on a hypothesis in which the double vacancy was assumed to have high mobility. The study of F-type centers has become more important since the last decade, because they have been found to have laser application. It is not the purpose of this thesis to track the whole history of F-type centers. In this chapter, we shall only mention some basic points, which are directly related to our present work. The interested reader may refer to the books of Fowler [3], Stoneham [4], and Farge and Fontana [5]. For another review of F-type centers, also see reference [6].

2.1 F Centers in Alkali Halides

The F center, which is an electron trapped in an anion vacancy (see figure 2.1), has been found to have an optical absorption band, called F absorption band or F

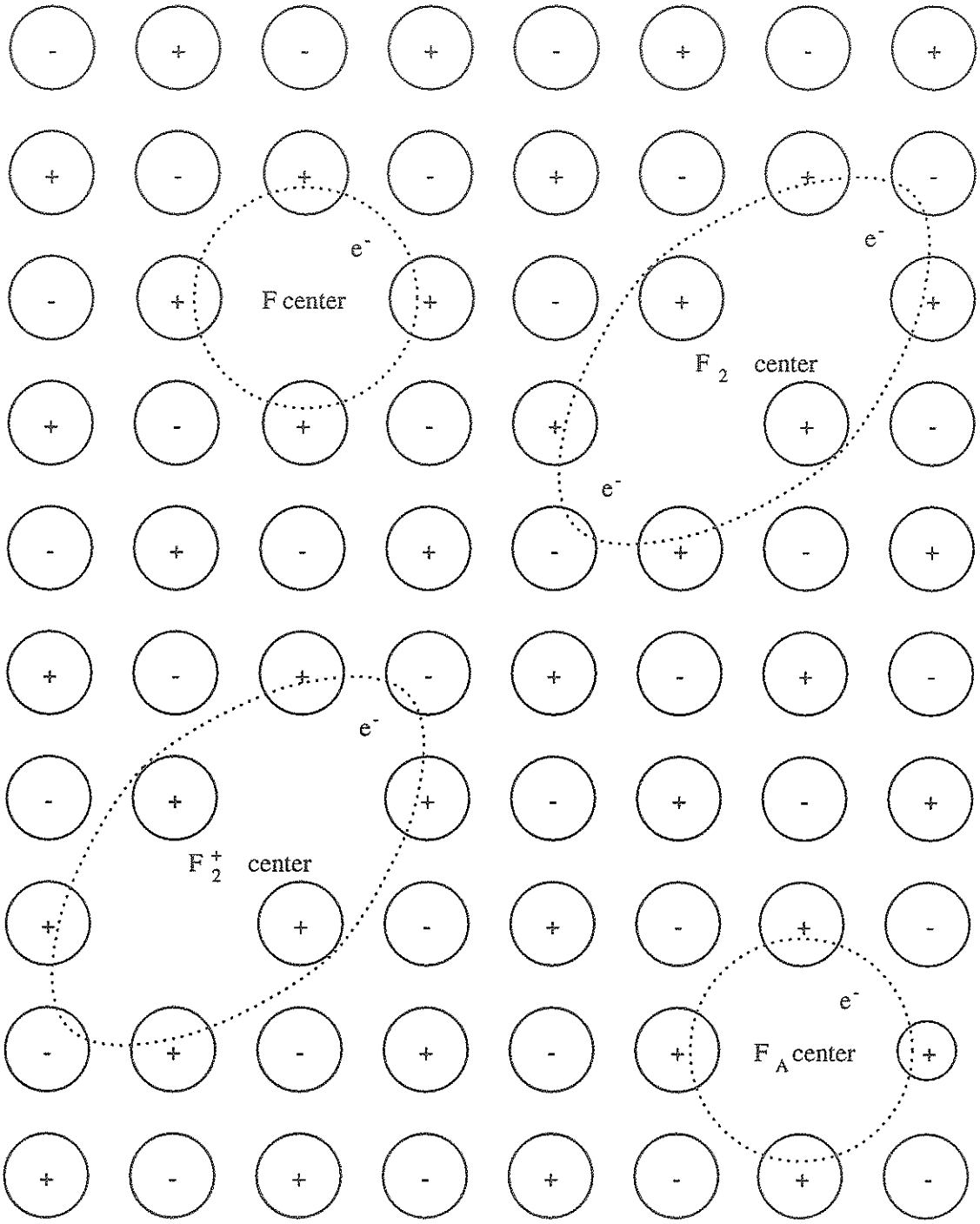

Figure 2.1: Common F-type centers in ionic crystals

band, and an emission band which is widely separated from the F band. Both of them are nearly of gaussian shape. In KBr [3], for instance, at 4 K, the F band is centered at 2.06 eV with a half-width of 0.16 eV. The corresponding emission band is located 1.14 eV away, at 0.92 eV, and has a half-width of 0.22 eV. Similar behaviors have been observed in most alkali halides, except for cesium halides [3, 7]. The optical cycle, the complete excitation/de-excitation process, of F centers consists of four subprocesses (see, for reference, Mollenauer and Pan [8]): (i) first, a photon is absorbed and the electron is excited into the absorption band from the ground state; (ii) then, the electron decays nonradiatively into the relaxed-excited state; (iii) this is followed by luminescence from the relaxed-excited state to the unrelaxed ground state; (iv) finally, the cycle is completed by another nonradiative decay back to the relaxed ground state. The most common physical model for the F band was that an electron is trapped by a three-dimensional potential well with a quasi-spherical symmetry. Then, the quantum states of the F center could be described by spherical harmonics, namely 1s, 2s, 2p etc. In the ground state, the electron is well confined in the vacancy. Therefore, for the F-absorption band, it would be a 1s-2p transition. This was followed by an empirical relation, the Mollwo-Ivey law [9],

$$E_F = 17.7a^{-1.84} \tag{2.1}$$

where, E_F, in units of eV, is the maximum F band energy for various alkali halides, and a, in Angström, is the perfect nearest anion-cation spacing. This relation shows good agreement with experiments [5]. However, no similar relation has been found for the emission band. This is thought probably because, in the emission process, the electron is not confined in the vacancy, but is more diffuse, moving in a Coulomb field with an effective mass m^* and an effective dielectric constant ϵ_∞ [10]. The Mollwo-Ivey law for the F band implies that there is a close relation between the dominant energies and lattice geometry [11].

The F center is of particular importance because it has a relatively simple structure, and it is the prototype of a variety of other color centers which can be obtained through F-center aggregation. For instance, with a nearest-neighbor host cation substituted by another alkali ion of smaller size, the F center becomes an F_A center, which has been found to have an important laser application that we shall discuss later. Two adjacent F centers form an F_2 center, formerly called M center, and further, if the F_2 center traps only one electron, it is an F_2^+ center, formerly called M^+ center, which is one of the focuses in the present work. Actually, the F center is not so easily studied. Its high-symmetry structure makes many physical measurements either difficult or even impossible. Another feature of the F center is that its coloration fades quickly at room temperature [3, 6]. Thus the hope for laser action in the F center is poor. F-center aggregates have therefore been considered, especially the impurity-doped ones. As with pure F-center aggregates, they will have the decreasing symmetry when defect size is increased during aggregation.

2.2 F-center Lasers

Laser operation has been found in many alkali halides [10, 11]. They are continuously tunable within a range from 0.8 μm to 4 μm (0.4 – 1.0 eV). Notice that the dye laser covers a range from the visible region to 1 μm, and on the other side, the Pb tunable diode laser is only good starting from 3 μm to longer wavelengths [10]. The very narrow linewidth of the F-center lasers also makes them valuable candidates for high-resolution spectroscopy [3, 10]. Another advantage is that F-center lasers have power output $A(P_{in} - P_{th})$ with low threshold P_{th} and high slope efficiency A such that they are very effective [11]. However, most of them cannot be turned into practical laser products since they are only stable at low temperature. Usually at room temperature, the laser effects disappear completely. One reason is that their relaxed excited states are too close to the conduction band ($\sim$ 0.1 eV [3, 10]).

Thus, thermal energy can easily raise the electron into the conduction band from the excited state. Until now, the only commercialized laser based on the F-center mechanism is the Burleigh FCL^{TM} laser, which provides continuous wave-tunable output from 2.2 μm to 3.3 μm with linewidth 1.5 GHz (single frequency 1 MHz) and output power 3 – 20 mw (2 – 15 mw). However, it is still unstable at room temperature.

The F_A center we mentioned earlier has been reviewed by Lüty [12]. In this center (see figure 2.1), with a nearest-neighbor host cation replaced by a smaller impurity alkali ion, the F-center's O_h symmetry is reduced to C_{4v}, which partially removes the triple degeneracy of the F band. In the F_A center, there are two polarized p-like transitions: one, named F_{A1}, is along the direction of the impurity ion; and the other, named F_{A2}, which is twofold degenerate, is perpendicular to that direction. Two types of F_A center have been found. Type I F_A centers, for example in KCl:Na^+, have properties similar to those of the F center. For type II F_A centers, which include the well-known center in KCl:Li^+, the emission band is broadly separated from the absorption band to the low-energy range and has a very narrow half width in comparison with those of F and F_A type I emissions. Experiments show that type II F_A centers cannot be easily ionized either by applying electric field or by increasing temperature. It was concluded by Lüty that there exists a considerably larger gap between the conduction band and the excited state of the type II F_A center than for the F center and the type I F_A center. These distinct behaviors favor the type II F_A center for laser application. Indeed, the first, and for a quite long period of time the only laser effect in F-type centers was observed in KCl:Li^+ by Fritz and Menke [6, 12].

Laser action from the F_2^+ center has been investigated extensively for a long time [3]. The most recent developments have been reported in references [13], [14] and [15]. The F_2^+ center (see also figure 2.1) is an ionized F_2 center, with an atom-

istic configuration of D_{2h} symmetry, oriented along the [110] direction. It has two absorption bands: one much like the F-center absorption band, and the other a low-energy band, which is not in the range of any other band of the F-type centers [15]. The F_2^+ center offers effective laser output with a range from 0.9 – 2 μm and nearly 100 % quantum efficiency [11, 13], and it was suggested by Mollenauer [13] to be suitable for practical laser products. However, the F_2^+ center is also unstable for continuous laser action. Its laser effects degrade very fast (reported from 15 minutes to several hours) at room temperature [15, 13]. Hofmann *et al* thought that the easy separation between two adjacent repelling anion vacancies (in NaF) could be one reason for this behavior.

2.3 The $(F_2^+)^*$ Centers in NaF

Improving the stability of the F-type-center laser operation at room temperature has been a long-time goal for researchers in this field. Although a great deal of effort was made, there was no significant improvement achieved until Mollenauer recently reported the discovery of a new kind of F_2^+-like center [16]. This center, named $(F_2^+)^*$ by Mollenauer, was found in rock-salt NaF doped with divalent impurities such as Mn^{2+}, Cr^{2+} or Ni^{2+} ions. It shows continuous wave-tunable laser effects with desirable quantum efficiency, and more important, much enhanced stability for several months at room temperature. Shortly later, Eisele *et al* carried out an investigation of $(F_2^+)^*$ centers in alkaline earth impurity-doped NaF [17]. It was found that in NaF doped with Mg^{2+} and Ca^{2+}, $(F_2^+)^*$ centers have even higher slope efficiencies (44 %) and lower threshold pump powers (30 mw and 45 mw, respectively) than those of the Mn^{2+}-doped $(F_2^+)^*$ center (24 % and 85 mw). They also have better stability at room temperature than the $(F_2^+)^*$ center in NaF: Mn^{2+}. These properties distinguish the $(F_2^+)^*$ centers from the other F-type centers found so far.

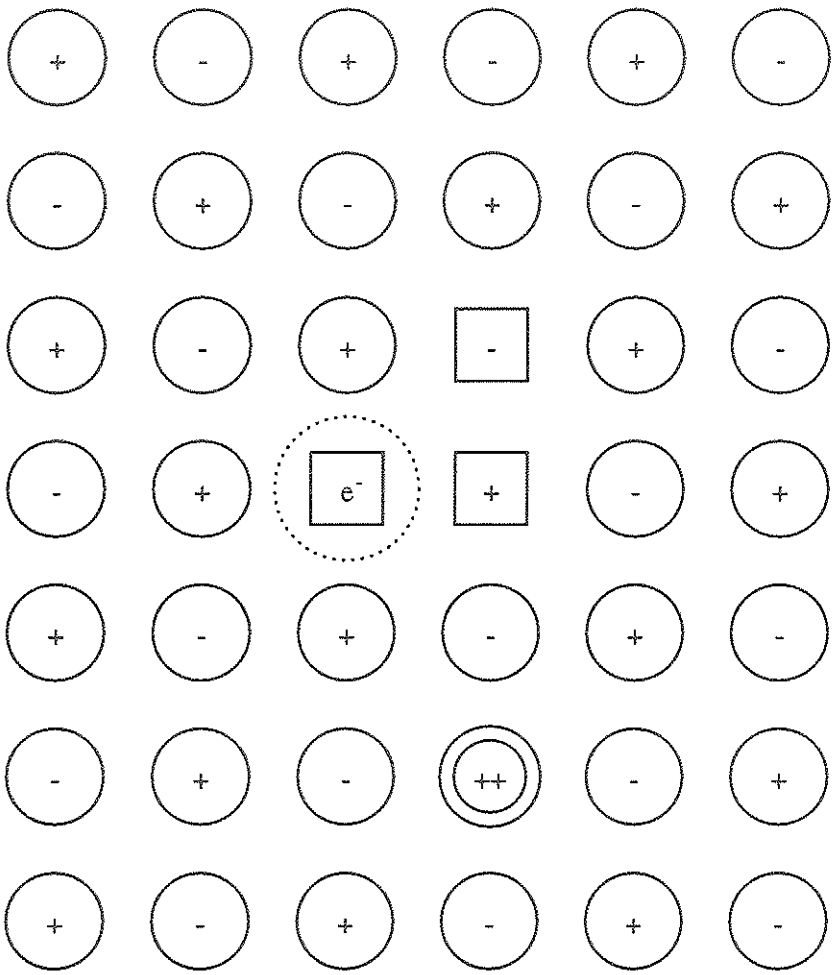

Figure 2.2: Hofmann model for the Mg^{2+} doped $(F_2^+)^*$ center in NaF

The $(F_2^+)^*$ center is a modified F_2^+ center, with a nearby divalent cation. It is not clear yet what the true mechanism is in its stabilization process, but experiments show that the $(F_2^+)^*$ center has almost the same absorption and emission bands (peak position, band shape and range) no matter what impurity is doped in NaF, and it is evident that the impurity plays a key rule in this process (whether as a stabilizer or as an electron trap is unknown) [17]. Consequently, this leads to investigation of the atomistic structure of the $(F_2^+)^*$ center. One of these attempts is the work of Hofmann and collaborators [15], in which they performed both experiments and theoretical simulations on the $(F_2^+)^*$ centers and obtained results similar to those of Mollenauer and Eisele *et al*. Hofmann *et al* then proposed a model for the atomistic structure of $(F_2^+)^*$ center. They also analyzed the F_2^+ center in the same host crystal since, on the one hand, this center is laser active itself, and on the other, it can provide useful information to compare with the $(F_2^+)^*$ center, due to the apparently close relation between two centers. Because our present work was initiated by the work of Hofmann *et al*, we briefly summarize their principal results below:

1 For the F_2^+ center in its ground state, in which an excess electron is equally shared by two anion vacancies, they found that most of the electron density is concentrated on the two Na^+ and four F^- ions in the plane between the two F^- vacancies. They inferred that the F_2^+ center has a more compact ground state than that for the F center.

2 For the $(F_2^+)^*$ center, they found that its ground-state structure is much like a single-vacancy F center rather than like the two-vacancy F_2^+ center. The excited $(F_2^+)^*$ state looks like that of a F_2^+ center.

3 It is still unknown what the true configuration is of the dipole formed by the Na^+ vacancy and divalent impurity in the $(F_2^+)^*$ center. However, from their experimental results and simulation, Hofmann *et al* considered the case where

the divalent cation is not adjacent to the Na^+ vacancy but dissociated. They also assumed that the Na^+ vacancy sits at the nearest-neighbor position of both anion vacancies of the F_2^+ center.

The objective of the present work is to further test the model of Hofmann *et al*. The previous work by Mollenauer and Eisele *et al* suggested that the atomistic structure of the $(F_2^+)^*$ center, especially the impurity configuration, would be a decisive point in the process of investigating the nature of the stability of this center. In the present work, we perform a series of simulations in a systematic way, using the ICECAP methodology, which is based on the unrestricted Hartree-Fock self-consistent field method with a shell-model lattice, to investigate both atomistic and electronic structures of the $(F_2^+)^*$ center. We consider Mg^{2+}-doped NaF, since previous investigations [15, 16, 17] have shown that the $(F_2^+)^*$ centers in NaF with different impurity doping display quite similar properties.

Chapter 3

Model Used for Simulation

In this chapter, we shall introduce the mathematical method and physical model used in the present work. In order to simulate a defect in the crystal lattice and investigate its physical properties, we look at the problem from a combination of quantum-mechanical and classical points of view. This is simply because only taking into account one of them will be either impractical or unrealistic. In section 3.1, we shall present the Hartree-Fock approximation method which is often used for the quantum-mechanical treatment of electronic problems. For this method, many text books and articles can be found (see, for example, reference [18]). Therefore, we only give a brief outline and general discussion. In section 3.2, we shall introduce the shell model which concerns a classical treatment of the crystal lattice. Those are two main concepts of the present work. In the last section, we summarize the program ICECAP which we have used in this simulation.

3.1 Hartree-Fock Self-Consistent Field Method

Generally, we are dealing with a many body problem when studying the nature of a defect in crystals. The alkali halide crystal lattice is an array containing cations and anions, consisting of nuclei and electrons. To describe such a system, the Hamiltonian will be very complicated, since many different kinds of motions and interactions are involved. Consequently, proper approximations are needed.

First, under the Born-Oppenheimer approximation, the static lattice approximation, the crystal can be seen as an array of ions with nuclei fixed at their lattice points and electrons which are moving in a potential field. If this is applied, the kinetic energy of nuclei can be dropped off from the Hamiltonian. Suppose there are N electrons and M nuclei in the crystal. Then the Hamiltonian of the system can be written as,

$$H = -\sum_{i}^{N} \frac{1}{2}\nabla_i^2 - \sum_{i}^{N}\sum_{j}^{M} \frac{Z_j}{|\mathbf{r}_i - \mathbf{R}_j|} + \frac{1}{2}\sum_{i}^{N}\sum_{i'}^{N} \frac{1}{|\mathbf{r}_i - \mathbf{r}_{i'}|} + \frac{1}{2}\sum_{j}^{M}\sum_{j'}^{M} \frac{Z_j Z_{j'}}{|\mathbf{R}_j - \mathbf{R}_{j'}|} \quad (3.1)$$

where, $\mathbf{r}_i$ and $\mathbf{R}_j$ are electron and nuclear position vectors, respectively; and Z_j are nuclear charges. The first term in equation (3.1) is the electron kinetic energy operator; and the other three terms are energy operators for electron-nuclear, electron-electron, and nuclear-nuclear Coulomb interactions.

In equation (3.1), we have used atomic units, in which the Planck's constant $\hbar$, the electronic charge e and the mass m are all set to unity. The energy is in units of Hartree, or a.u., and distance is in Bohr radius a_0. We shall use these units throughout this work. Explicitly, we have,

$$1 \text{ Hartree} = 2 \text{ Rydberg} = 27.2 \text{ eV}$$
$$a_0 = 0.529 \text{ Angström}.$$

Like in most quantum-mechanical problems, the next step we should follow is solve the Shrödinger equation with respect to the wave function Ψ which describes the whole system in a specific state. For a static lattice, consider the time-independent non-relativistic Shrödinger equation,

$$H\Psi = E\Psi \quad (3.2)$$

where, the Hamiltonian H is represented by equation (3.1), and E is the energy eigenvalue of H associated with the state Ψ of the system. Thus we first explore the nature of the solution Ψ. If we choose a complete orthonormal set of basis functions

Φ_i, denoted $|\Phi_i>$, then the solution Ψ, denoted $|\Psi>$, can always be expanded as,

$$|\Psi>=\sum_i C_i|\Phi_i> \tag{3.3}$$

where $C_i =< \Phi_i|\Psi >$ are the expansion coefficients of Ψ in terms of the basis set Φ_i. For the N-electron problem, with the requirement of the Pauli exclusion principle, it turns out that each Φ_i must be in the form of a Slater determinant, which is an antisymmetric product of N independent single-particle functions.

In the Hartree-Fock approximation, the basic idea is that one assumes that Ψ only contains one single Slater determinant. Therefore, denoted Ψ' now, we have,

$$\Psi' = (N!)^{-1/2} \begin{vmatrix} \phi_1(\mathbf{x}_1) & \phi_2(\mathbf{x}_1) & \cdots & \phi_N(\mathbf{x}_1) \\ \phi_1(\mathbf{x}_2) & \phi_2(\mathbf{x}_2) & \cdots & \phi_N(\mathbf{x}_2) \\ \vdots & & & \\ \phi_1(\mathbf{x}_N) & \phi_2(\mathbf{x}_N) & \cdots & \phi_N(\mathbf{x}_N) \end{vmatrix} \tag{3.4}$$

where, $(N!)^{-1/2}$ is a normalization factor; $\mathbf{x}_i$ represents both spatial coordinates $\mathbf{r}_i$ and spin coordinates s_i; and ϕ_i, $i = 1, 2, \cdots, N$, is a set of N orthonormal single-particle basis functions. At this stage, one can solve Shrödinger's equation (3.2) variationally by substituting equation (3.4). Now, our problem becomes finding a set of single-particle basis functions which satisfies the variational principle,

$$\frac{\delta}{\delta\phi_i}[< \Psi'|H|\Psi' >] = 0 \tag{3.5}$$

i.e. $< \Psi'|H|\Psi' >$ is a minimum. It is easy to see that this is still a quite difficult procedure to follow. Under the constraint that all the spin orbitals $|\phi_i >$ in a given single Slater determinant are orthonormal to each other, and with normalization of Ψ', the variational principle leads to the single-particle Fock equation (for detail, see reference [18]),

$$F\phi_i = \epsilon_i\phi_i \tag{3.6}$$

where, F is the Fock operator, and ϵ_i, $i = 1, 2, \cdots, N$, are its eigenvalues, or Fock energies, with respect to the Fock state ϕ_i. In equation (3.6), the Fock operator is

in the form,

$$F = -\frac{1}{2}\nabla^2 - \sum_{j=1}^{M} \frac{Z_j}{|\mathbf{r} - \mathbf{R}_j|} + \int d\mathbf{x}' \rho(\mathbf{x}', \mathbf{x}')|\mathbf{r} - \mathbf{r}'|^{-1} - \int d\mathbf{x}' \rho(\mathbf{x}', \mathbf{x})|\mathbf{r} - \mathbf{r}'|^{-1} P(\mathbf{x}, \mathbf{x}') \tag{3.7}$$

where, $P(\mathbf{x}, \mathbf{x}')$ is the interchange operator which operates on spatial-spin coordinates $\mathbf{x}$ and $\mathbf{x}'$, and $\rho(\mathbf{x}, \mathbf{x}')$ is the Fock-Dirac one-particle density operator which can be written as,

$$\rho(\mathbf{x}, \mathbf{x}') = \sum_{k=1}^{N} |\phi_k(\mathbf{x}) >< \phi_k(\mathbf{x}')| \tag{3.8}$$

In the single-particle Fock operator, equation (3.7), the last term is called the exchange interaction, due to exchanging spatial-spin coordinates between $\mathbf{x}$ and $\mathbf{x}'$. Since the Fock operator depends on its own eigenfunctions, the Fock equation (3.6) can only be solved iteratively. We rearrange equation (3.7), by putting the third and fourth terms together, as,

$$F = -\frac{1}{2}\nabla^2 - \sum_{j=1}^{M} \frac{Z_j}{|\mathbf{r} - \mathbf{R}_j|} + \int d\mathbf{x}' |\mathbf{r} - \mathbf{r}'|^{-1} \int d\mathbf{x}'' \delta(\mathbf{x}'', \mathbf{x}')[1 - P(\mathbf{x}, \mathbf{x}'')]\rho(\mathbf{x}', \mathbf{x}'') \tag{3.9}$$

Now in equation (3.9), the last term is called the self-consistent field because it represents the " field " which is seen by the ith electron and results from the $N - 1$ others. In order to solve the Fock equation, one first chooses an initial trial wave function and substitutes it into equation (3.9) to get a corresponding " field ". Then by solving equation (3.6), one obtains a new wave function. Following this routine repeatedly, one can make the self-consistency satisfied, and find the final eigenfunctions as well as the energy eigenvalues of the Fock operator. Apparently, there are many solutions that we can have. It all depends on how we choose the spin orbitals which construct the initial wave function.

Usually, two types of spin orbitals have been used. One is the restricted spin orbitals and the other is the unrestricted spin orbitals. In both of them, each spin orbital can be written in the form,

$$\phi_i(\mathbf{x}_i) = \phi_i(\mathbf{r}_i)\eta_i(s_i) \tag{3.10}$$

where, $\phi_i(\mathbf{r}_i)$ is the spatial orbital and $\eta_i(s_i)$ is the spin eigenfunction. For the restricted spin orbitals, the spatial orbital $\phi_i(\mathbf{r}_i)$ must satisfy the requirement of double occupancy. That is, for each $\phi_i(\mathbf{r}_i)$, there are two $\eta_i(s_i)$'s assigned — spin up and down. Therefore, N electrons in the system will fill up only $N/2$ spatial orbitals provided N is even. In the case of the unrestricted spin orbitals, the requirement is that each spatial orbital can only take the product with one of the spin eigenfunctions — spin up or down. This means that for spin up and spin down states, spatial orbitals may be different. These two different types of spin orbitals define two different methods — restricted and unrestricted Hartree-fock approximations.

Basically, there are two advantages in favor of the unrestricted Hartree-Fock method over the restricted regarding the cluster calculation: one is that the chemical bonds can dissociate properly; and the other is that electrons having opposite spins are allowed to correlate to each other [19]. Our present work is based on the unrestricted Hartree-Fock self-consistent field method. We shall see this point in section 3.3, where some further considerations, such as choosing the basis sets, will be given and in chapter 4, where we shall present specifically the problem we are studying and give the results. In the next section, however, we shall first introduce another approximation needed in our work — the shell model, which treats the crystal lattice classically, and therefore can be seen as complementing the unrestricted Hartree-Fock self-consistent field method in the present work.

3.2 Shell Model

The shell model was first developed by Dick and Overhauser [20] for classical treatment of the ionic crystals, which consist of polarizable cations and anions with opposite charges. This model has been used successfully to evaluate many physical properties of the ionic crystals and provides good agreements with the experimental results [23].

In the shell model, the short-range interactions among ions are considered pairwise and they can be described in terms of several parameters. Each ion with total charge Q is assumed to consist of two parts: a rigid shell with charge Y, and a rigid core with charge $(Q-Y)$. The mass of the ion is carried entirely by the core, and so the shell is considered massless. The shell and core of an ion are coupled harmonically through a spring such that the potential energy of the short-range interaction between them can be written as,

$$v(x) = \frac{1}{2}kx^2 \tag{3.11}$$

where k is the force constant and x is the shell-core separation. The short-range interactions between two ions are considered to act between their shells. In the original work of Dick and Overhauser, these interactions were also described in a harmonic form like equation (3.11). However in later work, it was found that they are better represented in the form of the Buckingham potential [23], which is anharmonic,

$$V(r) = Be^{-\frac{r}{\rho}} - \frac{C}{r^6} \tag{3.12}$$

where r is the shell-shell distance between two ions and ρ is the range constant. In equation (3.12), the first term represents the Born-Mayer repulsive interaction that is usually interpreted as overlap interaction between two ions; and the second term is the Van der Waals attractive interaction which results mostly from the correlation, or dispersion, effects [23]. All the ions, as point charges, experience Coulomb interactions with other ions. Therefore, in the shell model, we can use parameters k, Q, Y, B, ρ and C to describe the whole crystal classically. Many physical properties can be evaluated, such as elastic constant, dielectric constant, equilibrium configuration etc.

This model is of particular importance for the present work. One reason, as we mentioned earlier, is that it is not practical to treat the whole crystal quantum-mechanically. On the other hand, we also cannot treat the defect problem in a fully

classical way. Therefore, we can say that this model makes it practical for us to simulate a quantum-mechanical defect cluster embedded in the crystal lattice. The other reason is that it also makes it possible for us to further employ a simple model for investigating more complex defect problems, such as the $(F_2^+)^*$ center. We shall see this point in chapter 4.

3.3 ICECAP: Unrestricted Hartree-Fock Embedded-Cluster Computation

In this section, we describe the program used in the present work. This program, ICECAP, has been very successful in many point-defect calculations. The features of the program are fully discussed by Vail [22]. Here, we only describe some main points related to the present work.

3.3.1 Cluster Model

In the ICECAP method, the unrestricted Hartree-Fock self-consistent field method is used for the reason mentioned earlier in section 3.1. A defect cluster is chosen to include the excess electrons of the defect and ions perturbed both electronically and atomistically by the defect. All of these electrons and ions will be treated quantum-mechanically by the unrestricted Hartree-Fock self-consistent field approximation. At the same time, we consider the cluster embedded in an infinite classical crystal lattice described by the shell model, in which the ion-ion interaction is represented by the Coulomb potential and the shell-model short-range potential. The latter has the Buckingham form of equation (3.12).

Under the unrestricted Hartree-Fock self-consistent field approximation, the spin orbitals can be described by equation (3.10), in which spin eigenfunction $\eta_i(s_i)$ has either spin up or down. The way we solve the Fock equation (3.6) is still variational. We first have to choose the spatial orbitals $\phi_i(\mathbf{r})$. Generally, we can expand $\phi_i(\mathbf{r})$ in

terms of a linear combination of atomic orbitals $\chi_k(\mathbf{r})$,

$$\phi_i(\mathbf{r}) = \sum_{k=1}^{n} c_{ki}\chi_k(\mathbf{r}) \tag{3.13}$$

where, n is the number of atomic orbitals and c_{ki} are expansion coefficients. In equation (3.13), $\chi_k(\mathbf{r})$ are chosen to be gaussian-type functions (called primitive functions), since they are both computationally convenient and well localized. More specifically, we have,

$$\chi_k(\mathbf{r}) = N_k exp(-\alpha_k|\mathbf{r} - \mathbf{R}_j|^2)Y_l^m(\Omega_j) \tag{3.14}$$

where, α_k is the exponential coefficient of the gaussian function, N_k is the normalization factor, and Y_l^m is a spherical harmonic with angular dependence Ω. We can see from equation (3.14) that the gaussian function is localized at the site $\mathbf{R}_j$. Therefore, the molecular orbital $\phi_i(\mathbf{r})$ depends on a set of parameters α_k, (l, m, j) and coefficients c_{ki}. By substituting equations (3.13) and (3.14) into the Fock equation (3.6) while changing α_k and c_{ki} variationally, one could obtain the solution of the Hartree-Fock wave function by minimizing the total energy. This energy can be expressed in the form of the following three parts,

$$E_I = E_C + E_E + E_{INT} \tag{3.15}$$

where, E_C is the Hartree-Fock cluster energy, E_E is the environment, or embedding lattice, energy, and E_{INT} is the interaction energy between cluster and its environment. It is worth mentioning that the number of gaussian primitive functions, n, is also an important factor in this procedure. Its minimum is the number of electrons in the defect cluster. In principle, increasing n will bring higher accuracy. However, it also tremendously increases the computer time for the calculation due to the Hartree-Fock quantum cluster treatment. It is a practical question when one should stop raising n. It is also often impractical to variationally determine the α_k, since sometimes it means an unpredictable amount of computer time. Therefore in

practice, one usually takes the α_k from some other work. In the present work, the α_k and contraction coefficients are taken from Huzinaga [32]. The whole procedure mentioned so far in this section will be explicitly illustrated in section 4.2, where the ground states of the F and F_2^+ centers are studied.

Actually, some other aspects of the cluster model of the ICECAP method are not mentioned here. For instance, one might ask how an embedded quantum cluster can fit with an embedding classical shell-model lattice. It raises the problem of the cluster-lattice boundary conditions, mainly ion-size effect, i.e. the electronic structure of the embedding ions. This is completely ignored in the classical treatment of the embedding region. In ICECAP, this problem is dealt with by a procedure called Kunz-Klein localizing potential [21]. In the present work, we do not introduce the Kunz-Klein localizing potential. The effects among ions are taken into account by the shell model. Also, in our calculations, we do not include the correlation correction, which may be introduced into ICECAP to improve on the Hartree-Fock approximation. For details of the Kunz-Klein localizing potential and correlation correction, see, for example, reference [22].

3.3.2 The ICECAP Program

ICECAP, standing for Ionic Crystal with Electronic Cluster: Automatic Program, was developed in 1984 [24, 25] to carry out calculations of point and cluster defects in alkali halide crystals. It was designed as a user-friendly program with a highly-illustrative keyword-based input data format. ICECAP offers many options which make it suitable for a variety of applications. For instance, one can use it to simulate a defect cluster, which could be either a very complex impurity defect or a point defect with comparatively simple structure, like an F center. One also can use ICECAP for the perfect crystal. A variety of electronic and atomistic properties can be provided by ICECAP calculations.

The ICECAP program is constructed mainly from two other programs, namely HADES and UHF. HADES — Harwell Automatic Defect Examination System [26] — deals with an infinite crystal lattice containing a defect by using only the shell model. It can be used for many different types of the crystals and defects, with various choices of the form of the ion-ion short-range potentials. In the present work, the lattice geometry is FCC and the short-range potentials are chosen to be the Buckingham type (see equation (3.12)). In the HADES program, the crystal is divided into two regions — region I (inner region) and region II (outer region). Region I includes the defect cluster and a certain number of the neighboring ions. Its radius should be specified by the user. Region II extends to the entire infinite crystal. In the lattice relaxation process, HADES consistently and explicitly varies the core and shell coordinates of ions in region I to minimize the total energy until the equilibrium configuration is reached. Meanwhile, it treats the region II in the continuum approximation, i.e. electrostatic approximation. The lattice polarization is also taken into account. The region I is chosen by assigning a specific number of ions in the input data. The program will then determine the radius of region I accordingly. HADES provides many useful properties of the crystal, such as the shell-model energy E_H, elastic and dielectric constants, equilibrium atomistic configuration, and so on. On the other hand, the UHF program — Unrestricted Hartree-Fock, which was developed by Kunz *et al* [22] — treats the defect cluster region quantum-mechanically. Several requirements must be satisfied before UHF runs. We first have to specify the characteristics of the defect cluster. This includes its chemical structure and electronic features. Specifically, we must tell the program the nuclear charges and positions in the cluster, and the interactions between the cluster and the ions in the embedding crystal lattice. The basis sets also have to be specified. This means that the parameters $\alpha_k(l, m, j)$ in equation (3.14) should be assigned proper values. One also can use other options such as Kunz-Klein localizing

potential (see section 3.3.1). UHF then determines the energy eigenvalues ϵ_i and eigenvectors ϕ_i in equation (3.6) as well as the Hartree-Fock energy E_C in equation (3.15). It also provides a lot of other information about the electronic properties of the defect cluster, such as spin, Mulliken populations, multipole moments, and so forth.

In ICECAP, HADES and UHF are linked together along with the other auxiliary programs to complete the calculation automatically. For each cycle, first the charge distribution in the cluster is estimated and represented as point charges, HADES then fixes the defect cluster and relaxes the surrounding lattice by moving the shell and core positions of the neighboring ions, with polarization taken into account, to reach the minimum of the HADES energy E_H. Then, UHF is applied to the cluster to obtain the minimized Hartree-Fock cluster energy E_C and wave function Ψ' in terms of the electronic configuration while optimizing the coefficients c_{ki}. Note that corresponding to each step in the variation of the cluster atomic positions, UHF also performs a minimization. In doing so systematically and consistently, the final minimization of the total energy is reached.

Practically, in the ICECAP program, the total energy E_I is evaluated in a slightly different way than in equation (3.15). The HADES energy E_H is the classical shell-model energy for the whole lattice, in which the classical Coulomb energy W_C and the short-range interaction energy W_S for the cluster are already included in the Hartree-Fock cluster energy E_C. Therefore, these two parts are subtracted out from E_H when calculating the total energy E_I. That is, equation (3.15) now becomes,

$$E_I = E_C + E_{INT} + E_H - W_C - W_S \tag{3.16}$$

So far, we have only given a general outline of the ICECAP program. More specific features will be seen when particular problems are discussed in the next chapter.

Chapter 4

Methods and Results

Up to now in the previous chapters, we have given the general mathematical formulae and physical models as the background of the present work. In this chapter we shall further explore the particular methods and considerations that we need to accomplish our task. We shall also give the results of the calculations and discuss them in detail.

4.1 One-Electron Model for the $(F_2^+)^*$ Center

The $(F_2^+)^*$ center has a more complicated structure than other F-type centers do. We have not yet seen any theoretical investigation concerning the properties of the $(F_2^+)^*$ center, although some experimental work has been done.

The $(F_2^+)^*$ center consists of an F_2^+ center and an $Mg^{2+}{\cdot}V'_{Na}$ dipole. The F_2^+ center is formed by two adjacent anion vacancies. For the ground state of the $(F_2^+)^*$ center, Hofmann *et al* proposed a planar model in which the $Mg^{2+}{\cdot}V'_{Na}$ dipole points away from the F_2^+ center and is split (see figure. 2.2), with the cation vacancy staying at the nearest-neighbor position of both anion vacancies, and the excess electron localized in the anion vacancy which is closer to the doubly charged impurity cation (Mg^{2+}).

In order to investigate thoroughly the correctness of the Hofmann model and set up a firm foundation for further theoretical study of properties of the $(F_2^+)^*$ center,

one should consider other possible electronic and atomistic configurations, comparing their energies with each other and with the Hofmann model in a systematic way. However, the structure of the $(F_2^+)^*$ center is so complicated that to use the full power of the ICECAP methodology (see section 3.3), with adequate quantum clusters, would be prohibitively time consuming for us. For instance, even if we only simulate the Hofmann model, which is planar, not only shall we have a cluster with very low symmetry which is C_1, but also we will be dealing with a fairly large cluster, which includes two anion vacancies (an F_2^+ center), one cation vacancy (V'_{Na}), one doubly charged cation defect (Mg^{2+}) and at least their eighteen nearest-neighbor ions, of which half are Na^+ and half F^-. This cluster will contain 191 electrons. To determine the energy of a single configuration with that many electrons, and with self-consistently relaxed lattice, is a very large calculation. In addition, to complete the study of the structural model for the $(F_2^+)^*$ center, many other configurations need to be taken into account.

Therefore, to make this simulation more practical, but at the same time not lose too much its validity, we consider a more efficient and simpler model for the $(F_2^+)^*$ center. Once again, using the Hofmann configuration as an example, we consider a quantum-mechanical cluster that consists only of the trapped excess electron. All the ions of the crystal, including the Mg^{2+} impurity, are described by the shell model. Thus we shall have to deal only with a one-electron quantum-mechanical problem. Obviously, this one-electron model will significantly reduce the amount of calculation. However, before we apply this model to the simulation, there are some other important points which must be considered.

First of all, it is necessary to determine the shell-model short-range potentials. Many defect calculations in ionic materials [27, 28] have indicated that the quality of the potentials used to model the crystal lattice is a major concern in calculating the defect energy with high accuracy. In other words, we should be very careful in

dealing with these potentials.

Generally, there are two kinds of potentials in our $(F_2^+)^*$ center problem. The first is the interionic potentials. Most of them, such as those for Na^+-Na^+, Na^+-F^- and F^--F^- interactions, are the ionic potentials of the host crystal which can be obtained from previous study [30, 31]. In the present work, the parameters of these potentials, B, C and ρ in equation (3.12), have been taken from Catlow *et al* [30]. The only exception is the potential for interaction between the Mg^{2+} impurity and ions of the host crystal. Because Mg^{2+} is a tightly bound cation, it is usually assumed to be unpolarizable. That is, in the shell model, we see it as a point charge, or only as a core without a shell. For the same reason, we also neglect the interaction between the Mg^{2+} and its second nearest-neighbor ions, namely Na^+. As for the interaction between Mg^{2+} and F^-, MgF_2 does not have the rock-salt structure like our host crystal NaF, and its nearest-neighbor lattice spacing is totally different from that for NaF. The way we determine the Mg^{2+}-F^- short-range potential is by using the ICECAP method. That is, we put Mg^{2+} in a cluster that includes its six nearest-neighbor F^- ions, and carry out an embedded quantum-mechanical cluster calculation. We will come back to this point in the next section.

The second kind of potential must express the F-center interactions with Na^+ and F^- ions, as well as with the Mg^{2+} impurity. Although there has been a variety of quantum cluster calculations involving F-type centers in alkali halides, they do not consider the equivalent pairwise classical potentials of the F center-ion interactions. In the present work, we assume that F center-ion short-range potentials have the Buckingham form. Then we determine these potentials from large embedded quantum-mechanical cluster calculations. We will discuss this in more detail in section 4.4.

We also investigate the possibility of scaling the F center-Na^+ potential to apply it to the F_2^+ center. When this is found to fail, new potentials are derived for F_2^+-ion

interactions. There remains the question of the compatibility of these derived F- or F_2^+-center potentials with the varying configurations studied for the $(F_2^+)^*$ center. This point will be discussed in section 4.5.

4.2 Short-range Potential: NaF: Mg^{2+}

In this section, we shall derive the Mg^{2+}-F^- short-range potential. The method is originally from Pandey and Vail, who have used it for hydrogen anions in MgO [29].

Because we have ignored the polarization and second nearest-neighbor interaction of the Mg^{2+}, we now only have to take an $(Mg^{2+})(F^-)_6$ cluster (see figure 4.1), which has 70 electrons treated quantum-mechanically in the UHF-SCF cluster calculation, to derive the nearest-neighbor short-range Mg^{2+}-F^- interaction by using the ICECAP program. The basic idea in this method is that we use a shell-model cluster to simulate the corresponding Hartree-Fock quantum cluster. Both of them are embedded in the identical classical NaF shell-model crystal. We first assume that in NaF, the Mg^{2+} cation interacts with its six nearest-neighbor F^- anions similarly as it does in MgF_2, following equation (3.12) which is of the Buckingham type. Equation (3.12) can be re-written as,

$$V(B, C, \rho; r) = Be^{-\frac{r}{\rho}} - \frac{C}{r^6}. \tag{4.1}$$

We are going to determine B, C and ρ by varying r. Further, we let

$$E_I(r) = E_H(r) - 6V(B_0, C_0, \rho_0; r) + 6V(B, C, \rho; r) + k \tag{4.2}$$

where, $E_I(r)$ is the ICECAP (total) energy, $E_H(r)$ is the shell-model energy, which we will call the HADES energy because it is calculated by the HADES program [26], B_0, C_0 and ρ_0 are the short-range parameters for Mg^{2+}-F^- interaction for MgF_2, and k is a renormalization factor. Note that HADES is part of ICECAP, so we just take the HADES energy from the ICECAP output, and do not have to run it separately.

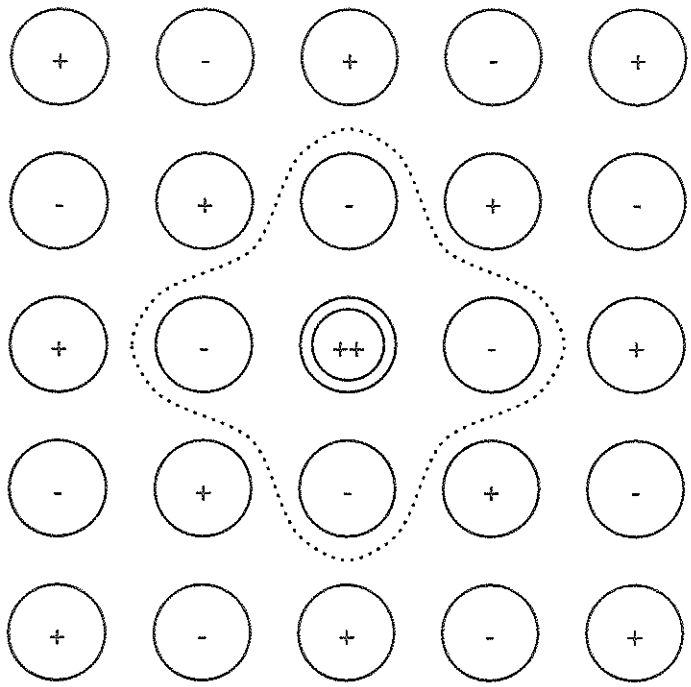

Figure 4.1: The nearest-neighbor cluster for NaF: Mg^{2+}

Table 4.1: Parameters of the Buckingham short-range potentials for NaF crystal: taken from Catlow *et al* [30].

	B (eV)	ρ (Å)	C (eVÅ^6)
Na^+ - F^-	1594.2	0.2555	0.0
Na^+ - Na^+	7895.4	0.1709	11.68
F^- - F^-	1127.7	0.2753	11.68

To get a fit for the parameter set B, C, ρ and k from equations (4.1) and (4.2), we define a new function,

$$f_i(B, C, \rho, k) = 0 \tag{4.3}$$

with

$$f_i = E_I(r_i) - E_H(r_i) + 6V(B_0, C_0, \rho_0; r_i) - 6V(B, C, \rho; r_i) - k \tag{4.4}$$

where, $i = 1, 2, 3, 4$, corresponding to four different r values which we need to solve equation (4.3) for B, ρ, C and k.

In the calculations, actually we have taken five r values, to fit the potential more accurately about the equilibrium position. We compress and enlarge the cluster through moving its six nearest-neighbor F^- ions inward and outward about the equilibrium positions in the range of 20 percent of the perfect lattice spacing. Then we have five equation (4.3)'s in terms of r_i, where $r_1 = 0.80a$, $r_2 = 0.85a$, $r_3 = 0.90a$, $r_4 = 0.95a$ and $r_5 = 1.00a$. Notice that a is the perfect lattice spacing of the NaF crystal, being taken as 2.295 Å. The parameters of the shell-model potentials of the host crystal are taken from reference [30], shown in table 4.1. Gaussian basis sets for Mg^{2+} and F^- are obtained from Huzinaga [32], both of them with (43/4) contraction. For Mg^{2+}, actually we have used the free Mg set. The basis sets are shown in tables 4.2 and 4.3. We judge the fit obtained by solution of equation (4.3) by considering

$$s = \sum_i^5 |f_i|^2, \tag{4.5}$$

and require $s \leq 10^{-2}$ (eV)^2. In table 4.4, we list the energies E_I and E_H calculated

Table 4.2: Contracted basis set for Mg^{2+}: taken from the free Mg (43/4) set of Huzinaga [32]. The exponential coefficient α is in Bohr atomic units a_0^{-2}.

Orbital	α	Contraction
1s	1894.17840000	0.0188745
	285.51327000	0.1310931
	64.27509900	0.4577639
	17.10119200	0.5308957
2s	25.82549500	−0.0885017
	2.39817270	0.5838364
	0.81951998	0.4933946
2p	50.71731100	0.0403941
	11.43098500	0.2236495
	3.23696950	0.5120981
	0.92860588	0.4443718

Table 4.3: Contracted basis set for F^-: taken from the free F^- (43/4) set of Huzinaga [32]. The exponential coefficient α is in Bohr atomic units a_0^{-2}.

Orbital	α	Contraction
1s	1040.66250000	0.0192338
	156.68433000	0.1333205
	35.11987900	0.4609976
	9.29325510	0.5266653
2s	13.98919800	−0.0797469
	1.16228750	0.5838995
	0.32317710	0.5075939
2p	19.10617300	0.0523561
	4.14631680	0.2585270
	1.07208680	0.5082607
	0.23984997	0.4634154

Table 4.4: ICECAP energy E_I and HADES energy E_H for the $(Mg^{2+})(F^-)_6$ cluster: both are in units of eV. The separation of Mg^{2+} and F^-, r, is in units of NaF nearest-neighbor spacing.

r	E_I	E_H
0.80	−21629.42	−14.47
0.85	−21630.69	−15.54
0.90	−21630.74	−15.69
0.95	−21630.05	−15.16
1.00	−21628.88	−14.15

Table 4.5: The parameters of the Mg^{2+}-F^- shell-model interaction:
a. taken from Mackrodt and Stewart [31] for MgF_2.
b. derived from cluster calculation.

	B (eV)	ρ (Å)	C (eVÅ^6)
a	4378.43	0.22614	0.4393
b	24671.69	0.1847	0.0

with ICECAP for the $(Mg^{2+})(F^-)_6$ cluster embedded in the relaxed NaF shell-model lattice. The equilibrium nearest-neighbor distance for this cluster is found to be 0.89 a. In the fitting, we find that we can only get the best fit with $C = 0$ (if $C \neq 0$, we have very large s). This means that the Mg^{2+} cation interacts with the host F^- anions in the form of the Born-Mayer potential. In table 4.5, we give the results from the fitting, together with the Mg^{2+}-F^- interaction parameters for MgF_2 taken from reference [31], for comparison.

From table 4.5, one can see that the short-range interaction between the Mg^{2+} impurity and its nearest-neighbor F^- anions in NaF is quite strong, but the range of the interaction is slightly shorter than that in MgF_2.

4.3 F and F_2^+ Centers: Ground States

We now analyze the F and F_2^+ centers, which are two basic elements of our $(F_2^+)^*$ problem. In this section, we determine the basis sets and equilibrium configurations

of these two centers in their ground states in NaF. In the next section, we shall derive the short-range potentials between each of them and host ions, as well as the F center-Mg^{2+} potential.

4.3.1 The F Center

The work of Pandey and Vail [29] indicates that in MgO, although the F center is fairly well localized in the anion vacancy, its wave function is relatively diffuse. They found that the defect's properties are sensitive to the defect basis sets and lattice relaxation. In our analysis for the F center in NaF, we first consider a nearest-neighbor $(Na^+)_6$(F center) cluster (see figure 4.2) to determine the F-center basis set. Then we enlarge it to a second nearest-neighbor $(Na^+)_6(F^-)_{12}$(F center) cluster (see figure 4.3) and optimize the the F-center basis set in this cluster. These two clusters have the same symmetry. There are 61 quantum-mechanical electrons in the former case but 181 in the latter. Finally, we calculate the equilibrium configurations of the second nearest-neighbor defect cluster embedded in the NaF shell-model crystal.

To determine the F-center primitive functions in NaF, we need the exponential coefficients α of its gaussian-type orbitals. We keep the F center basis set uncontracted throughout our work. In the nearest-neighbor $(Na^+)_6$(F center) cluster, we have taken the F center orbital to be of s type. We estimate an initial value of α using following equation,

$$R = (2\alpha)^{-1/2} \tag{4.6}$$

where, R, in units of NaF perfect lattice nearest-neighbor spacing, is the range of the orbital. If we let $R = 0.5\ a$, we obtain α approximately with the value of $0.1\ a_0^{-2}$, where a_0 is the Bohr atomic radius. For the six nearest-neighbor Na^+ ions, we use the free Na^+ basis set from Huzinaga [32], with (43/4) contraction, shown in table 4.6. We execute a series of UHF-SCF cluster calculations by using

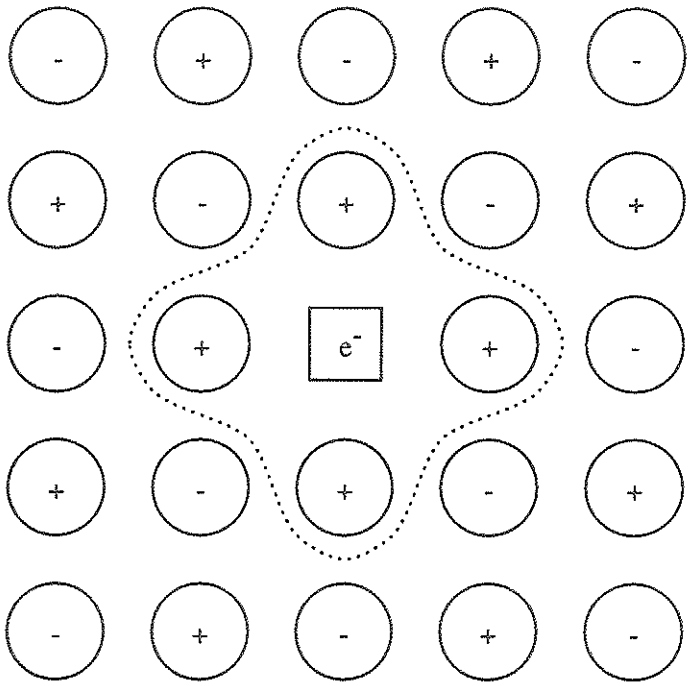

Figure 4.2: The nearest-neighbor cluster for the F center in NaF

Table 4.6: Contracted basis set for Na^+: taken from the free Na^+ (43/4) set of Huzinaga [32]. The exponential coefficient α is in Bohr atomic units a_0^{-2}.

Orbital	α	Contraction
1s	1562.63160000	0.0192363
	235.88220000	0.1329870
	53.17220000	0.4600791
	14.15975900	0.5269627
2s	21.42552200	−0.0856725
	1.93426680	0.5778588
	0.62799346	0.5024330
2p	38.80258600	0.0427562
	8.67551940	0.2304547
	2.41015550	0.5105285
	0.65992043	0.4488300

ICECAP program, while keeping six Na^+ neighbors at their perfect lattice positions and varying α of the F-center basis set to minimize the total energy. Table 4.7 gives the results from these calculations, including the optimized α and total energy.

Then we add a second s orbital to the F-center basis set and perform the same calculations. We fix α_{s1} at 0.08 a_0^{-2} while varying α_{s2} to obtain minimized total energy. In table 4.8, we give the results of these calculations. In comparison with

Table 4.7: Total energy E, in units of eV, calculated for the $(Na^+)_6$(F center) cluster: with the F-center (1/0) set and the Na^+ (43/4) set (see table 4.6). The exponential coefficient α of the F-center basis set is in Bohr atomic units a_0^{-2}.

α	E
0.10	−26354.44
0.09	−26354.49
0.08	−26354.48
0.0872976	−26354.50†

† Optimized values

Table 4.8: Total energy E, in units of eV, calculated for the $(Na^+)_6$(F center) cluster: with the F-center (11/0) set and the Na^+ (43/4) set (see table 4.6). The exponential coefficient α is in Bohr atomic units a_0^{-2}. The α_{1s} for the F-center basis set is fixed at 0.08.

α_{2s}	E
0.20	−26354.52
0.10	−26354.53
0.06	−26354.51
0.1351180	−26354.53†

† Optimized values

Table 4.9: Contracted Na 3s orbital: taken from the free Na (433/4) set of Huzinaga [32]. The exponential coefficient α is in Bohr atomic units a_0^{-2}.

Orbital	α	Contraction
3s	0.52440000	−0.1133903
	0.05407000	0.7008421
	0.02106000	0.3743411

the case of a single s orbital, we see that adding a second s orbital to the F-center basis set only lowers the total energy about 0.03 eV.

Another key point that we want to know is whether the F-center electron is mainly localized at the center of the vacancy, or is occupying the Na 3s orbitals. Many previous investigations on the F-center electronic properties assumed the former. To investigate this, it is necessary to add the 3s orbital to the Na^+ basis set and see where the excess electron tends to go by looking into the Mulliken populations from the ICECAP calculation. In order to make this simple and still comparable with the calculations done without the Na 3s orbital, we do not use the complete Na (433/4) basis set, which is also available from reference [32], but only add its 3s orbital to the Na^+ (43/4) set. Table 4.9 lists this Na 3s orbital basis set. We only carry out one single calculation for the purpose of comparison. We use the F-center (1/0) basis set at the vacancy. The total energy lowering from the extra

Table 4.10: Mulliken populations calculated for the $(Na^+)_6$(F center) cluster: with the Na^+ (43/4) and (433/4) basis sets. For the F-center (1/0) basis set, α is taken to be 0.09.

	Na^+ (43/4) basis set		Na^+ (433/4) basis set	
	spin up	total	spin up	total
F center	1.0000	1.0069	0.8834	0.8913
Na^+1s	1.0000	2.0000	0.9999	1.9998
Na^+2s	1.0000	1.9997	0.9992	1.9981
Na^+3s	–	–	0.0213	0.0228
Na^+2p	1,0000	1.9992	0.9994	1.9982
	1,0000	2.0000	0.9998	1.9996
	1,0000	2.0000	0.9998	1.9996

Na 3s orbital is 0.22 eV. In table 4.10, we give the Mulliken populations from both Na^+ (43/4) and Na (433/4) basis sets. We see that with the Na 3s orbital available, the excess electron still shows a strong tendency to stay at the vacancy site. The Na 3s orbital only reduces the Mulliken population of the spin up state of the excess electron at the center by 12 percent, of which each of the six nearest Na^+ neighbors is responsible for 2 percent. The total population at the center is also reduced by about the same amount. So, introducing the Na 3s orbital does not result in much charge transfer from the defect center to its six nearest Na^+ neighbors.

From all of above, we believe that for the present simulation on the F center in NaF, there is no need for including the second F-center s orbital or the Na 3s orbital. It is sufficient to use only the F-center (1/0) and the Na^+ (43/4) basis sets for our further cluster calculations.

We are now in a position to analyze the ground state properties for the F center in the second nearest-neighbor cluster. In this quantum cluster (see figure 4.3), we use the Na^+ (43/4) contractions (see table 4.6) for the six nearest-neighbor Na^+ ions and the F^- (43/4) contractions (see table 4.3) for the twelve second nearest-neighbor F^- ions. In order to investigate the distortion field and the equilibrium configurations of

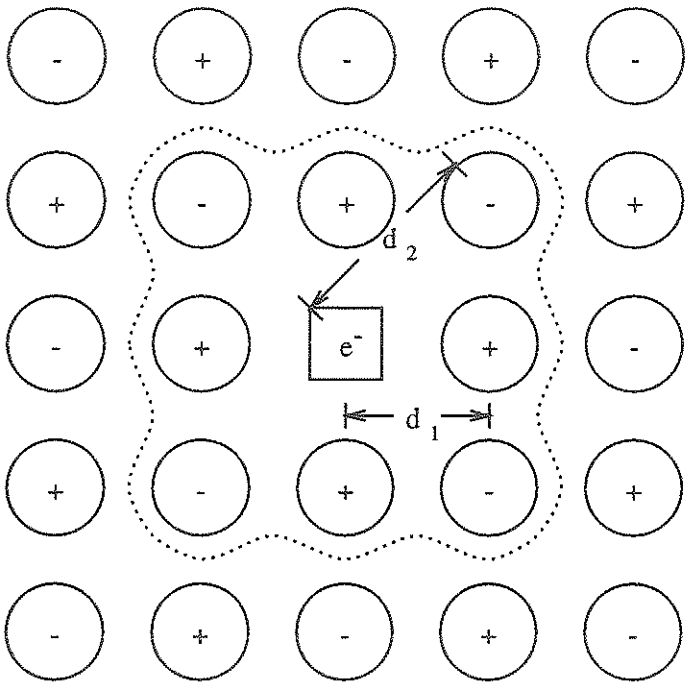

Figure 4.3: The second nearest-neighbor cluster for the F center in NaF

Table 4.11: Minimized total energy E_I, for the ground state of the F center in the second nearest-neighbor cluster: corresponding to the F-center-nearest-neighbor ion distance d_1 and the F-center-second-nearest-neighbor ion distance d_2, both in units of perfect lattice nearest-neighbor spacing a, and the optimized exponential coefficient α.

d_1 (a)	d_2 (a)	α (a_0^{-2})	E_I (eV)
0.70	1.41	0.1769869	−58784.56
0.90	1.41	0.1141181	−58794.31
1.00†	1.41	0.0940154	−58795.14
1.10	1.41	0.0773169	−58794.28
1.20	1.41	0.0555198	−58792.00
1.00	1.31	0.0957267	−58793.46
1.00	1.36	0.0949671	−58794.74
1.00	1.40‡	0.0941722	−58795.16
1.00	1.41	0.0940154	−58795.14
1.00	1.46	0.0930410	−58794.31
1.00	1.51	0.0925192	−58793.01

† Equilibrium position for the nearest-neighbor ions
‡ Equilibrium position for the second nearest-neighbor ions

the defect crystal, we shall compress and enlarge the cluster by varying the nearest-neighbor and second nearest-neighbor positions. This is a similar procedure as in the previous section for deriving the Mg^{2+}-F^- potential, but here at every position we optimize the exponential coefficient α by varying it to get the minimized total energy of the defect lattice. First, we fix the second nearest-neighbor F^- positions and move the nearest-neighbor Na^+ ions. We compress the cluster by 30 percent and enlarge it by 20 percent of the perfect lattice spacing. Then, the nearest-neighbor Na^+ ions are held at their perfect lattice positions and the F^- ions are moved inward and outward by about 7 percent. We choose the large displacements so that the results can be used in the next section to derive effective potentials. Table 4.11 gives the minimized total energies and corresponding optimized α's in terms of the different F center-ion distances. The equilibrium distances of the nearest-neighbor ions and of the second

Table 4.12: Mulliken populations for the ground state of the F center: second nearest-neighbor cluster.

	spin up	total
F center	1.0000	1.0128
Na^+1s	1.0000	2.0000
Na^+2s	1.0000	1.9998
Na^+2p	1.0000	1.9991
	1.0000	2.0000
	1.0000	2.0000
F^-1s	1.0000	2.0000
F^-2s	1.0000	1.9999
F^-2p	1.0000	1.9998
	1.0000	1.9998
	1.0000	2.0000

nearest-neighbor ions are also presented. We find the nearest-neighbor equilibrium positions almost at their perfect lattice positions (displaced inward 0.0001 a) and the second nearest-neighbor equilibrium positions slightly inward (0.01 a) from their perfect positions. The total relaxation energy of these displacements is only 0.02 eV. In table 4.12 we show the Mulliken populations obtained for this second nearest-neighbor cluster. Only (-0.01) electron charge is found to transfer into the defect center from the neighboring ions. In conclusion, we find that, although the F center is quite flexible and polarizable, in this high-symmetry ground-state configuration, it is strongly localized in the defect center and produces negligible distortion. These properties may not prevail, however, in lower-symmetry states.

4.3.2 The F_2^+ Center

We now explore the F_2^+ center ground state. This center has a lower symmetry (D_{2h}) than the F center because it consists of two vacancies along the [110] direction. If we still consider a second nearest-neighbor cluster as before, it will contain 10

nearest-neighbor Na^+ ions and 18 second nearest-neighbor F^- ions, with a total of 281 quantum electrons. Such a large, low-symmetry cluster would be very time-consuming to analyze using ICECAP. Thus we consider a nearest-neighbor cluster (see fig 4.4), which only consists of 10 Na^+ ions and 101 quantum electrons.

The procedure of analyzing the F_2^+ center is almost the same as that we used earlier for the F center. We first keep the nearest-neighbor Na^+ ions at their perfect lattice positions and optimize the F_2^+ center basis set. Then the parameters of the basis set are fixed at the optimized values and we vary the nearest-neighbor positions to minimize the total energy of the defect lattice. At the same time, the HADES part of ICECAP relaxes the rest of the lattice and determines the ion positions. There are three inequivalent sets of nearest neighbors. For each set, we vary the positions of these nearest-neighbor ions in a systematic way. For instance, we take one step outward in one direction, say x, and then take several steps(inward and outward) one by one in the other two directions, namely y and z. Next we move the x position again. When we obtain the relaxed configuration and corresponding minimized total energy of the defect lattice, we keep the nearest-neighbor ions at their relaxed positions and re-optimize the basis set. Iterating this, we get the finally relaxed lattice configuration and the minimized total energy of the defect lattice.

In this calculation, we use the same basis set for the Na^+ ions as before. For the F_2^+ center, there are two possibilities to be considered. One is that, with the F-center electron shared between two vacancies, it may be necessary to add a 2p gaussian orbital to the F-center (1/0) basis, to have a (1/1) basis set. The other is with the F-center electron at the saddle point, the 1s and 3d orbitals will need to be considered, giving a (1/0/1) basis set. Table 4.13 shows the results for these two cases. There are only coordinates for three nearest-neighbor ions shown in the table since all ten can be sorted into these three groups. In table 4.14, we give the Mulliken populations from the (1/1) set calculation. Table 4.15 is for the case

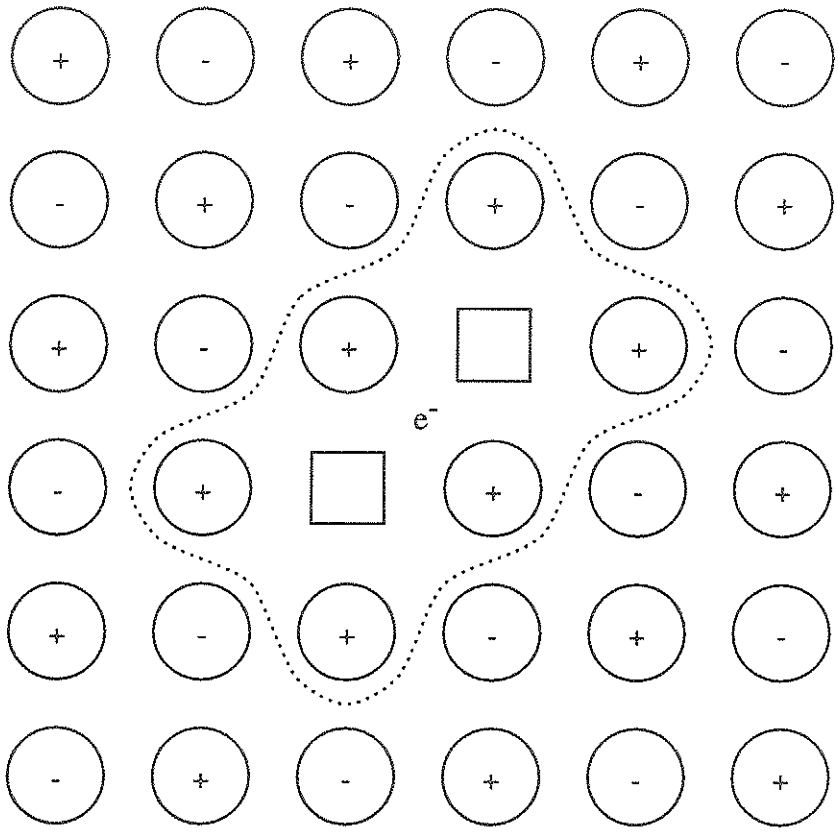

Figure 4.4: The F_2^+ center in NaF: nearest-neighbor cluster

Table 4.13: The ground-state results for the F_2^+ center in nearest-neighbor cluster: minimized total energy E_I (eV), relaxation energy ΔE (eV), optimized α (a_0^{-2}), relaxed F center distance d (a) and nearest-neighbor coordinates of the relaxed configuration x, y, z (a), for basis set (1/1) at the two vacancies, and for basis set (1/0/1) at the saddle point (origin).

	α_s	α_p	α_d	E_I	ΔE	d	x	y	z
(1/1)	0.09	0.11	–	−43935.45	0.34	1.33	0.55	−0.55	0.00
							0.49	1.55	0.00
							0.49	0.49	1.05
(1/0/1)	0.13	–	0.09	−43834.63	0.35	–	0.50	−0.50	0.00
							0.50	1.55	0.00
							0.50	0.50	1.08

Table 4.14: Mulliken populations for the F_2^+ center with (1/1) basis set in each vacancy, unrelaxed and relaxed configurations.

	Unrelaxed		Relaxed	
Orbital	spin up	total	spin up	total
F center 1s	0.4609	0.4688	0.4676	0.4735
F center 2p	0.0291	0.0363	0.0239	0.0298
	0.0291	0.0363	0.0239	0.0298
	0.0070	0.0139	0.0058	0.0114

Table 4.15: Mulliken populations for the F_2^+ center with (1/0/1) basis set at the saddle point, unrelaxed and relaxed configurations.

	Unrelaxed		Relaxed	
Orbital	spin up	total	spin up	total
F center 1s	0.6413	0.6495	0.6115	0.6190
F center 3d	0.1218	0.1283	0.1276	0.1334
	0.1218	0.1283	0.1276	0.1334
	0.0797	0.0845	0.1009	0.1056
	0.0585	0.0622	0.0534	0.0564
	0.0065	0.0128	0.0059	0.0116
	0.0065	0.0128	0.0059	0.0116

of the (1/0/1) set. From these tables, it can be seen that for both cases, the defect lattice gains almost the same amount of energy lowering (0.34 – 0.35 eV) through lattice relaxation. However, for the (1/1) set, the total energy of the defect lattice is about 0.82 eV lower than that for the (1/0/1) set. In the case of the (1/1) set, two saddle-point ions are spread out by about 5 percent of the nearest-neighbor lattice spacing in both x and y directions. The remaining 8 nearest-neighbor ions are also moved out by 5 percent in only one direction (x, y or z). The centers of the two lobes of the F-center wave function move closer to each other by about 6 percent.

In conclusion, the F_2^+-center electron is split between the two vacancies, rather than localized at the saddle point. Because of the net positive charge, the nearest neighbors are forced outward by 5 to 7 percent of the perfect lattice nearest-neighbor distance. From table 4.14, we see about (-0.09) charge transfer into the center from its nearest neighbors, with about (-0.14) charge in overlapping p-type orbitals from the two vacancies.

4.4 Classical Potentials for the F-type Centers

Before we can start investigating the $(F_2^+)^*$ center using the one-electron model, we must obtain all the short-range potentials for interactions between the F-type centers and ions in the crystal. First we derive the F center-host ion potentials.

In the previous section, we have calculated the total energies of the defect lattice in terms of the different nearest-neighbor and second nearest-neighbor distances as well as the optimized exponential coefficient α (see table 4.11), where the nearest-neighbor and second nearest-neighbor ions were included in the quantum-mechanical cluster. Now, we consider the quantum cluster to consist only of the F-center electron trapped in the defect vacancy. This will have ICECAP treat the 6 nearest-neighbor cations and 12 second nearest-neighbor anions as shell-model ions rather than quantum-mechanically. We take the same nearest-neighbor and second nearest-

neighbor distances as in the many-electron cluster calculations and keep each α corresponding to each distance at its optimized value as determined in the many-electron (large cluster) case. In this way, we can have 5 one electron energies (E_{1e}) corresponding to 5 large cluster energies (we still call them E_I). The latter are taken from table 4.11, and one-electron energies are shown in table 4.16. We assume that the potentials have the Born-Mayer form (see equation (3.12)) and derive them by fitting the coefficients B and ρ. However, we then obtain results with $s \gg 10^{-2}$. After carefully analyzing the data, we carry out another fit in terms of the Buckingham potential (see equation (4.1)). For this calculation, equation (4.2) becomes

$$E_I(r) = E_{1e}(r) + 6V(B_1, C_1, \rho_1; r_1) + 12V(B_2, C_2, \rho_2; r_2) + k \qquad (4.7)$$

where subscripts 1, 2 are referring nearest-neighbor and second nearest-neighbor interactions, respectively. This time, the convergence criterion for s is fully satisfied. The fitting results are given in table 4.17. It can be seen that the Born-Mayer interactions between the F center and the host ions are much like the ion-ion interaction, but the attractive forces are much stronger. The repulsive interaction between the F center and second nearest F^- neighbors is stronger, and longer-ranged, than that between the F center and the nearest-neighbor Na^+ ions.

Next, we determine the interactions between the F_2^+ center and the host ions. We still assume a form of pairwise short-range potential. However, we first consider simply scaling the potentials that we have just obtained for the F center. From the symmetry and the work we reported in the previous section, we assume that the F_2^+ center is formed by two adjacent F centers, each containing only half an electron, and we therefore scale the point charge they share and the short-range parameters B and C for the F center by 0.5, but keep ρ unchanged. Then, we perform a one-electron calculation using ICECAP and vary the distance between two half F centers to find the minimized total energy in the relaxed lattice configuration. If the scale

Table 4.16: One-electron energy E_{1e} for the F-center ground-state calculations: corresponding to the F center-nearest-neighbor ion distance r_1 and the F center-second-nearest-neighbor ion distance r_2, both of which are in units of perfect lattice nearest-neighbor spacing a, as well as the exponential coefficient α.

r_1 (a)	r_2 (a)	α (a_0^{-2})	E_{1e} (eV)
0.70	1.41	0.1769869	7.29
0.90	1.41	0.1141181	3.22
1.00	1.41	0.0940154	2.94
1.10	1.41	0.0773169	3.75
1.20	1.41	0.0555198	5.49
1.00	1.31	0.0957267	4.50
1.00	1.36	0.0949671	3.43
1.00	1.41	0.0940154	2.94
1.00	1.46	0.0930410	3.42
1.00	1.51	0.0925192	4.35

Table 4.17: The parameters of the F center-Na^+ and the F center-F^- potentials: derived from the many-electron quantum-cluster calculations.

Interaction	B (eV)	ρ (Å)	C (eVÅ^6)
F center-Na^+	4493.82	0.27484	212.199
F center-F^-	7272.47	0.37117	2073.114

Table 4.18: The parameters of the F_2^+-host ion potentials: obtained from 0.5 scaled potential parameters for F center-host ion short-range interactions (see table 4.17) with ρ kept unchanged.

Interaction	B (eV)	ρ (Å)	C (eVÅ^6)
F_2^+-Na^+	2246.91	0.27484	106.099
F_2^+-F^-	3636.24	0.37117	1036.557

Table 4.19: One-electron results for the F_2^+ center with the F-center potentials scaled by 0.5, F-center basis set (1/1): minimized total lattice energy E_{1e} (eV), relaxation energy ΔE (eV), optimized α (a_0^{-2}), relaxed F center distance d (a) and nearest-neighbor coordinates of the relaxed configuration x, y, z (a).

α_s	α_p	E_{1e}	ΔE	d	x	y	z
0.09	0.11	−4.88	0.11	1.27	0.50	−0.50	0.00
					0.50	1.51	0.00
					0.50	0.50	1.01

we have chosen is physically correct, the one-electron result should provide a lattice configuration and variations of the total energy with nearest-neighbor distances which are close to the 101-electron (nearest-neighbor quantum cluster) results. The scaled potential parameters are shown in table 4.18. The calculated total energy, nearest-neighbor positions and equilibrium F-center distance are given in table 4.19. Comparing the one-electron results with those of the 101-electron calculation in table 4.13, we see that the nearest-neighbor relaxations differ significantly in the two cases. This indicates that the short-range potentials we used for the F_2^+ center by scaling 0.5 are not correct. We then explore the possibility of other scales. Even though we do obtain a one-electron lattice configuration very close to the many-electron one for F center-Na^+ scaling of 0.68 and F center-F^- scaling of 0.5, we are still not satisfied with the variation of the total energy with nearest-neighbor distances, which is completely different from the result in the many-electron case. Finally, we have therefore had to re-derive the F_2^+-host ion potentials. We keep the

Table 4.20: One-electron and 101-electron results for re-deriving the F_2^+-Na^+ potential parameters: one-electron total energy E_{1e} (eV), many-electron total energy E_I (eV), F center distance d (a) and nearest-neighbor position coordinates d_i (a).

E_{1e}	E_I	d	d_1	d_2	d_3	d_4	d_5
−1.77	−43935.42	1.33	0.53	0.49	1.53	0.49	1.03
−1.61	−43935.45	1.33	0.55	0.49	1.55	0.49	1.05
−1.35	−43935.36	1.33	0.57	0.49	1.57	0.49	1.07

Table 4.21: The short-range parameters for the F_2^+-Na^+ and the F center-Mg^{2+} interactions in NaF.

Interaction	B (eV)	ρ (Å)	C (eVÅ^6)
F_2^+-Na^+	914.36	0.27484	12.476
F center-Mg^{2+}	16.07	1.2201	0.0

scale for the F center-F^- potential at 0.5 since we believe that it is less important, and we only re-derive the F center-Na^+ potential. From table 4.13, it can be seen that in the many-electron calculation, the equilibrium lattice relaxation has three of the five independent nearest-neighbor position coordinates relaxed by 5 percent, while the other two, d_2 and d_4, are hardly displaced at all. Then fixing d_2 and d_4 at 0.5 distance between the two half F centers as found for equilibrium relaxation, we carry out several large-cluster and one-electron ICECAP calculations, varying the other d's as a single variable. We fix the exponential coefficients α_s and α_p at the values found earlier for the F_2^+ center-Na^+ interaction, and determine B and C by fitting the two total-energy curves. The results are shown in table 4.20. From these data, following the same procedure for determining the potential parameters before, we obtain the new parameters for the F_2^+-Na^+ potential, which are given in table 4.21.

The last short-range potential needed for our (F_2^+)*-center analysis is the F center-Mg^{2+} interaction in NaF. For this purpose, we consider a quantum cluster (see

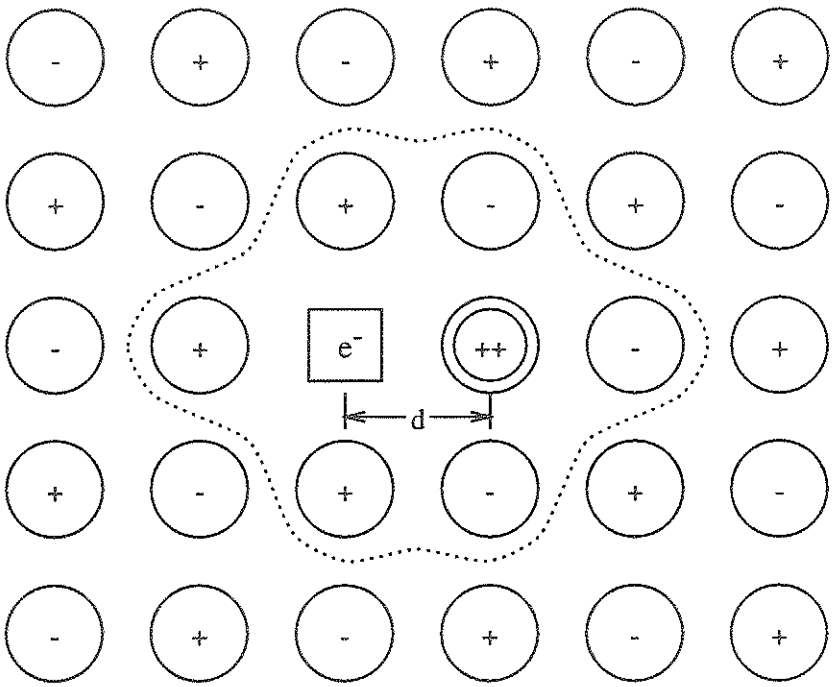

Figure 4.5: The nearest-neighbor cluster for deriving F center-Mg^{2+} interaction

Table 4.22: Many-electron results for the $(Mg^{2+})(F^-)_5$(F center)$(Na^+)_5$ cluster: total defect lattice energy E_I (eV), and optimized α (a_0^{-2}) in terms of the different F center-Mg^{2+} distances d (a).

d	α_s	α_p	E_I
0.90	0.100	0.12	−40902.41
0.95	0.095	0.11	−40902.55
1.00	0.090	0.10	−40902.62
1.05	0.090	0.10	−40902.63
1.10	0.090	0.09	−40902.57

figure 4.5), in which the F center and Mg^{2+} cation are at nearest-neighbor positions to each other, and they are surrounded by 5 nearest-neighbor Na^+ and 5 nearest-neighbor F^- ions. This requires a relatively large cluster calculation due to both the number of the electrons (111) in the cluster and the gaussian primitive wave functions involved. For Na^+, F^- and Mg^{2+}, we use (43/4) basis set, taken from tables 4.6, 4.3 and 4.2, respectively. For the F center, a (1/1) set is used. We minimize the total energy by varying the F center-Mg^{2+} distance in the range of 10 percent nearest-neighbor spacing inward and outward, at the same time optimizing the exponential coefficients α of the F-center basis set at each step. Then, several one quantum-electron calculations are carried out at the same F center-Mg^{2+} distances, maintaining the optimized α values found in the large-cluster calculations. The results of the total energy and α are shown in table 4.22. The potential parameters obtained from fitting are listed in table 4.21. It turns out that the interaction between the F center and Mg^{2+} impurity in NaF has the Born-Mayer form with weak repulsive force but quite long range in comparison with Na^+-F center and F^--F center interactions. So it may or not be that important for some configurations in our investigation on the $(F_2^+)^*$ center later in the next section.

4.5 One-Electron Results for the $(F_2^+)^*$ Center

In the previous sections of this chapter, we have analyzed the F-center and the F_2^+-center ground states. We have also obtained the short-range classical potentials for interactions between the F-type centers and ions, as well for the Mg^{2+}-F^- interaction in NaF. These provide us with a good foundation to investigate a number of possible configurations of the $(F_2^+)^*$ center by using the one-electron model, which treats only the excess electron trapped in the F_2^+ center quantum-mechanically and all the ions, including the Mg^{2+} impurity, by the shell model. In the present investigation, we select out some possible configurations and compare them, including the Hofmann model, using the one-electron model to predict the most stable configuration.

In their work, Hofmann *et al* considered the case that for the Mg^{2+} doped $(F_2^+)^*$ center in NaF, the Mg^{2+}·V'_{Na} dipole, in which Mg^{2+} and V'_{Na} are dissociated, and the F_2^+ center are coplanar. In the present work, we concentrate mainly on some planar configurations and a few nonplanar ones. Specifically, in addition to the Hofmann model (see figure 2.2), we consider 7 planar configurations and 3 nonplanar ones, which are shown in figures 4.6 to figure 4.15. We label all these configurations from 1 to 11, starting from the Hofmann model. They include every case with V'_{Na} at the nearest-neighbor position of both anion vacancies, including the dipole split to a distance of 2 a. Our coordinate system is shown in figure 4.6, with two anion vacancies at $(-1,0,0)$ and (0,1,0), labeled as site a and site b, respectively. In the calculation, the short-range parameters for the host ion-ion interactions are taken from table 4.1, and for the Mg^{2+}-F^- interaction from table 4.5. The parameters for interactions between the F-type centers and ions are obtained from tables 4.17, 4.18 and 4.21. Note that for the F-type center-Na^+ interaction, there are two possibilities. One is that in a symmetrical configuration, the excess electron is shared equally by two vacancies, so the short-range parameters for the F_2^+-Na^+ interaction (table 4.21)

should be used. Also, we should use the F-center (1/1) basis set for this case. The other is when the electron is localized at one of the two vacancies, for which we should use the potential for the F center-Na^+ interaction (table 4.17) and the F-center (1/0) basis set.

We first carry out a one-electron ICECAP calculation for each of these 11 configurations, using the proper potentials and basis set. Then for those with low-lying total energies, we further minimize their total energies by relaxing the centers of the electron orbitals. Table 4.23 summarizes the results from these calculations. In the first column, we list the labels for all 11 atomistic configurations. The sublabels, a and b, refer to two different electronic configurations, in which the excess electron is localized at vacancy center a or b (see figure 4.6) in a symmetry-broken configuration. For a symmetric configuration of the ions, such configurations 2, 5 and 11, we also calculate one of these two cases to test the energy lowering due to the symmetry breaking. The next two columns give the V'_{Na} and Mg^{2+} atomic positions. The fourth column is the total ICECAP energy and the fifth gives the energy lowering obtained from the relaxation of the F-center basis set centers. Column six is the Mulliken population. Note that for center a or b localization, we have $P_M = 1$, but for the cases in which the excess electron is equally shared by two centers, we have $P_M = 0.5$ for both of them. The following three columns show the same physical properties as column 4, 5 and 6 except that they are for the calculations with a reduced region I. This is required because, for the three nonplanar configurations, we have encountered a problem due to the lower symmetries, and been forced to reduce the size of region I. Region II is also modified correspondingly. To gain a better comparison among all the configurations, we have redone the calculations for the planar cases in the reduced region. Comparing the results for the different region sizes, we see no significant changes except for configurations 2 and 5, both of them having symmetrical configurations. Nevertheless, these two cases are not that

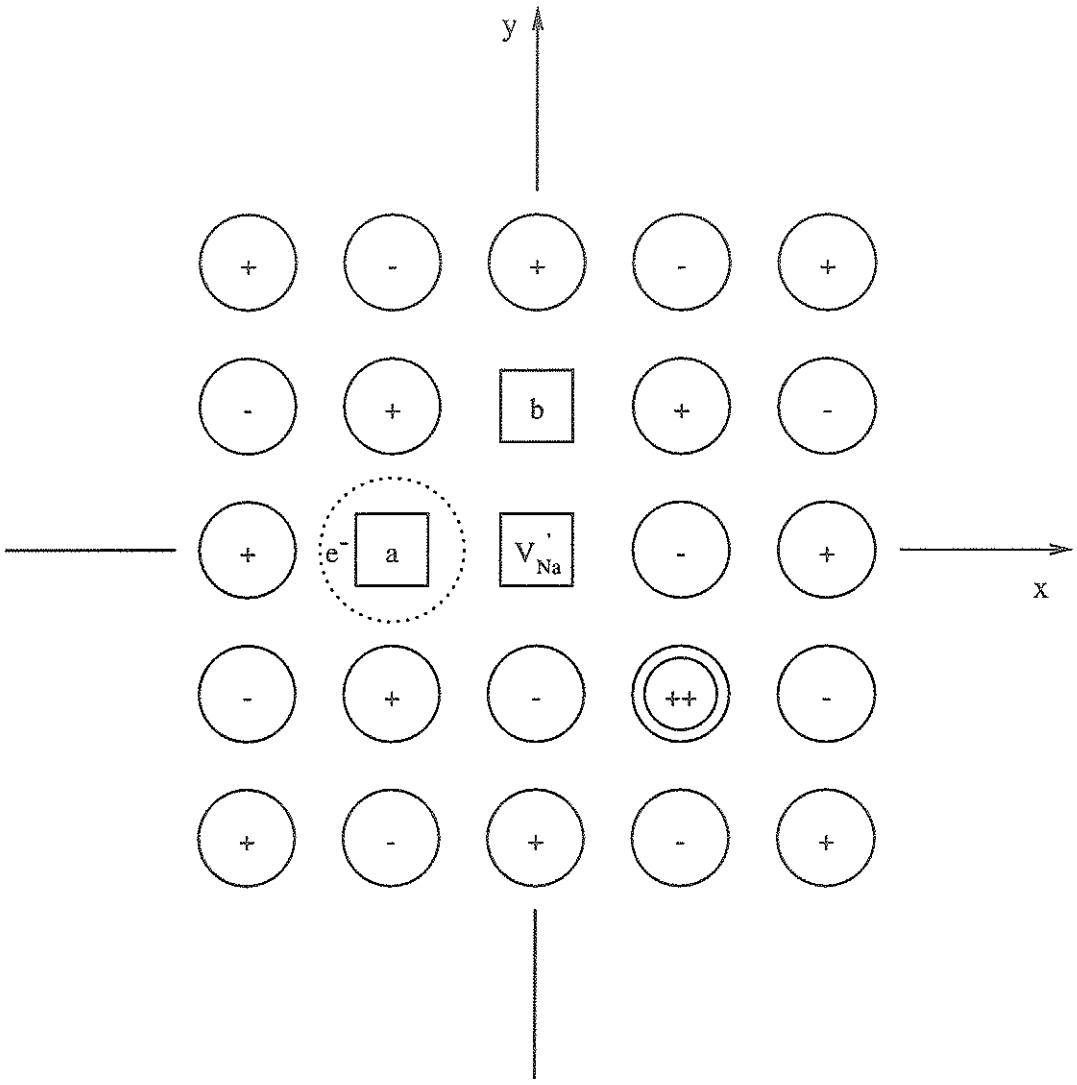

Figure 4.6: The $(F_2^+)^*$ center: configuration 2

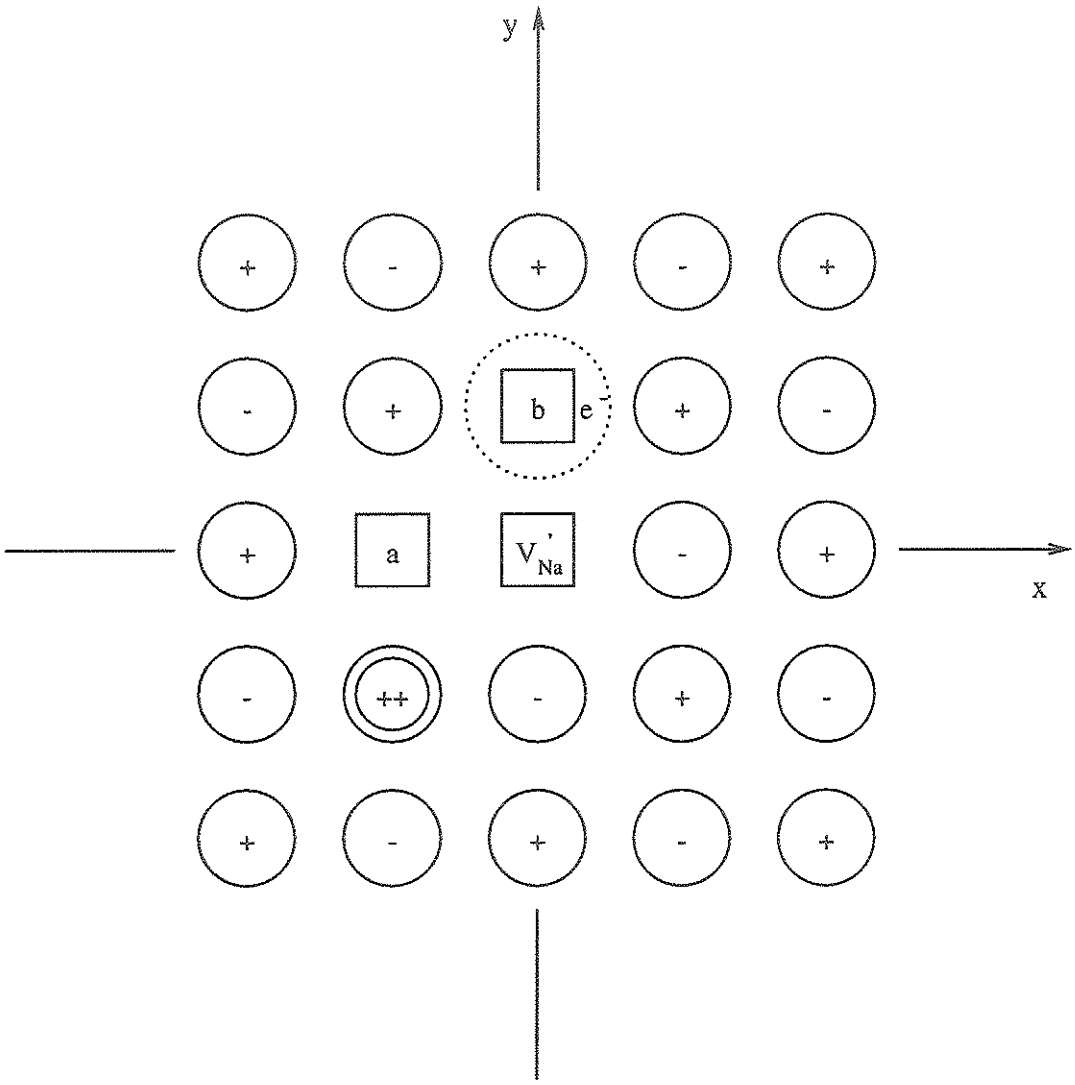

Figure 4.7: The $(F_2^+)^*$ center: configuration 3

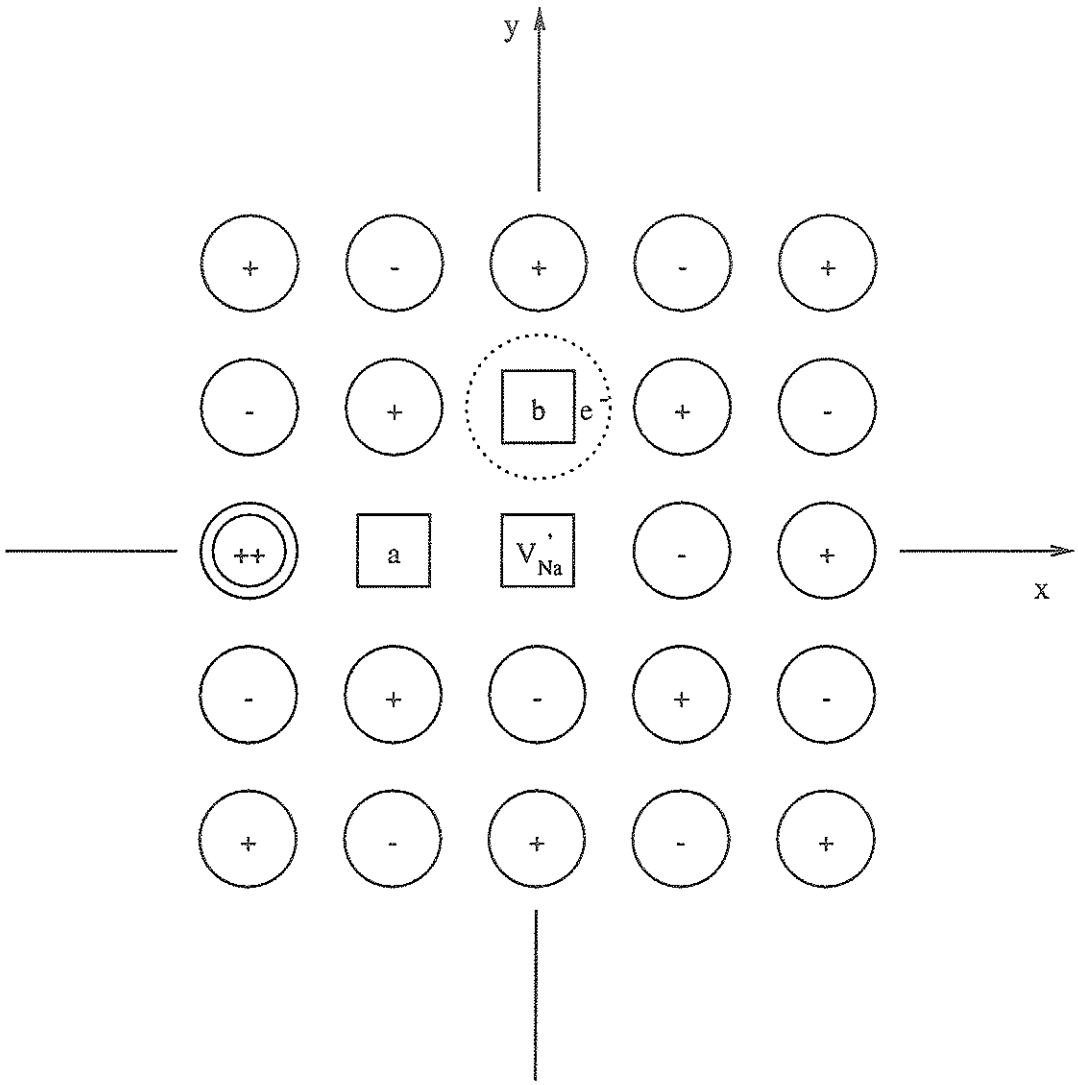

Figure 4.8: The $(F_2^+)^*$ center: configuration 4

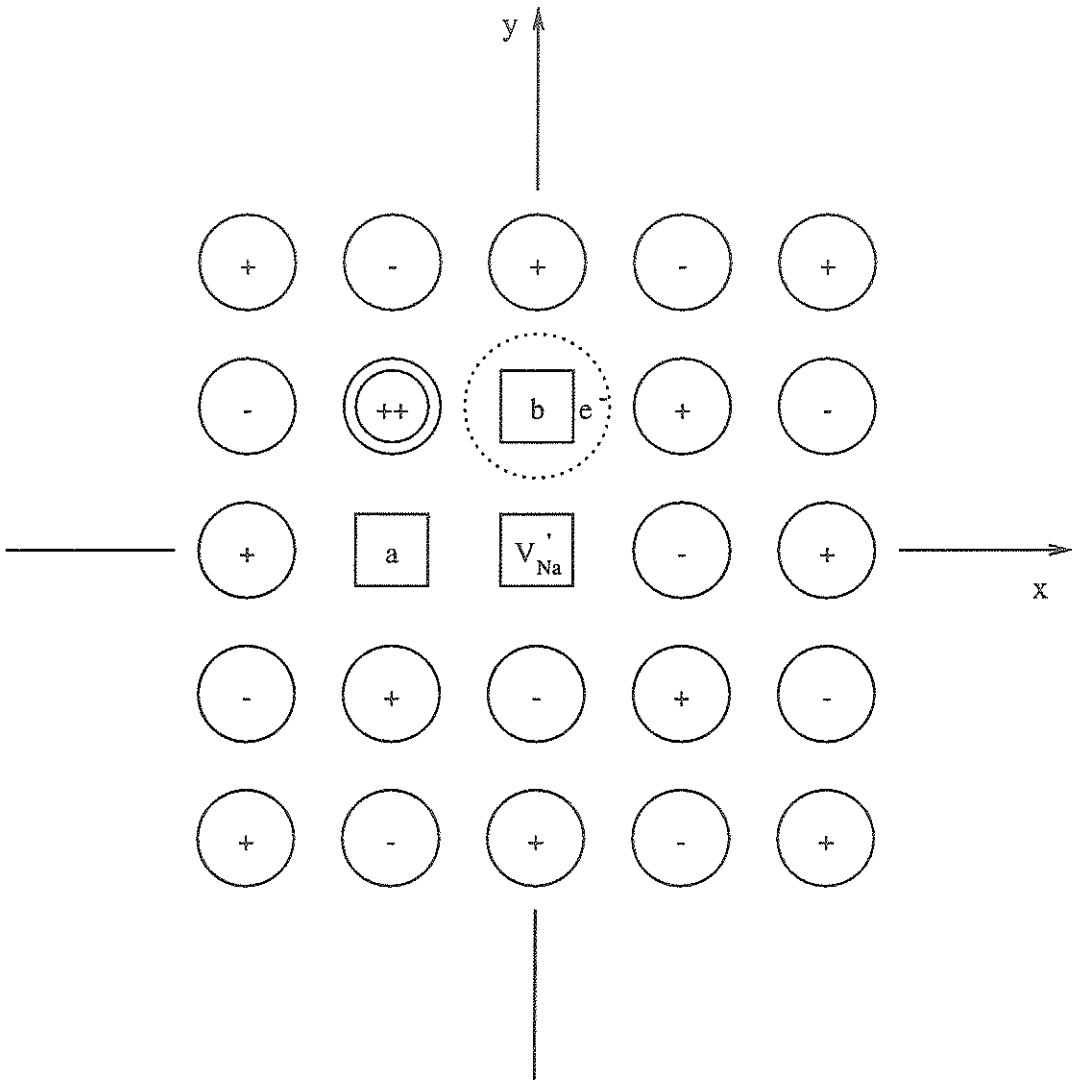

Figure 4.9: The $(F_2^+)^*$ center: configuration 5

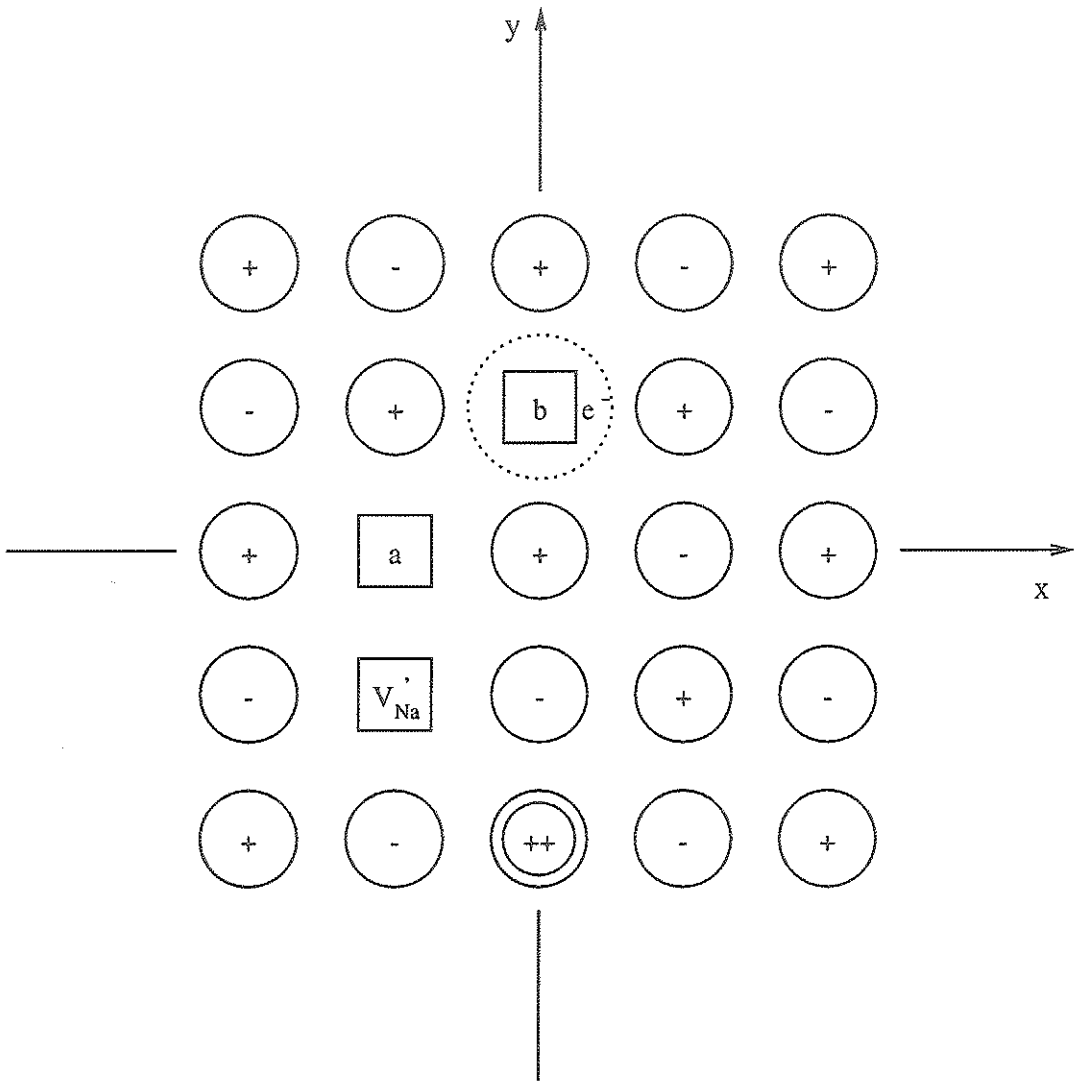

Figure 4.10: The $(F_2^+)^*$ center: configuration 6

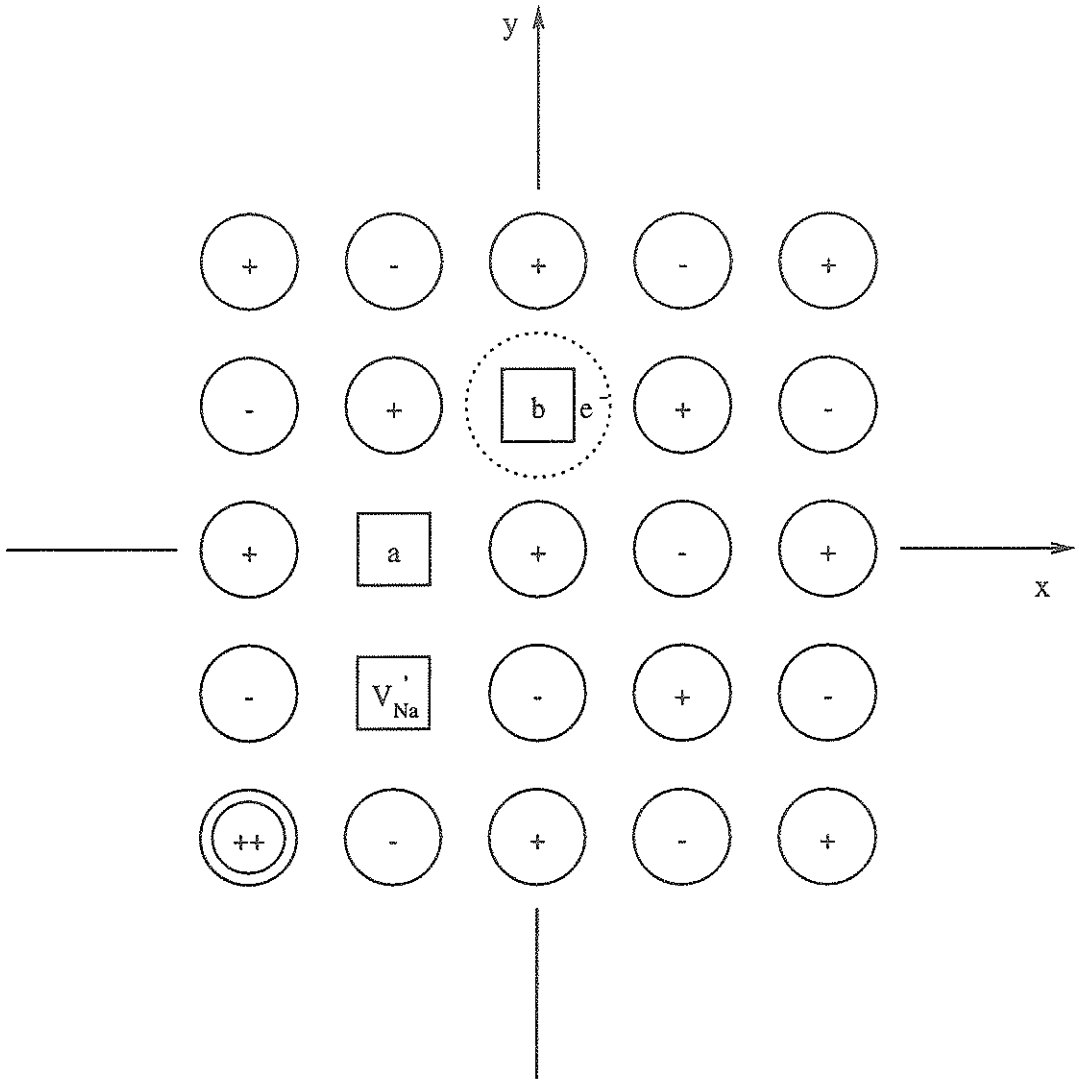

Figure 4.11: The $(F_2^+)^*$ center: configuration 7

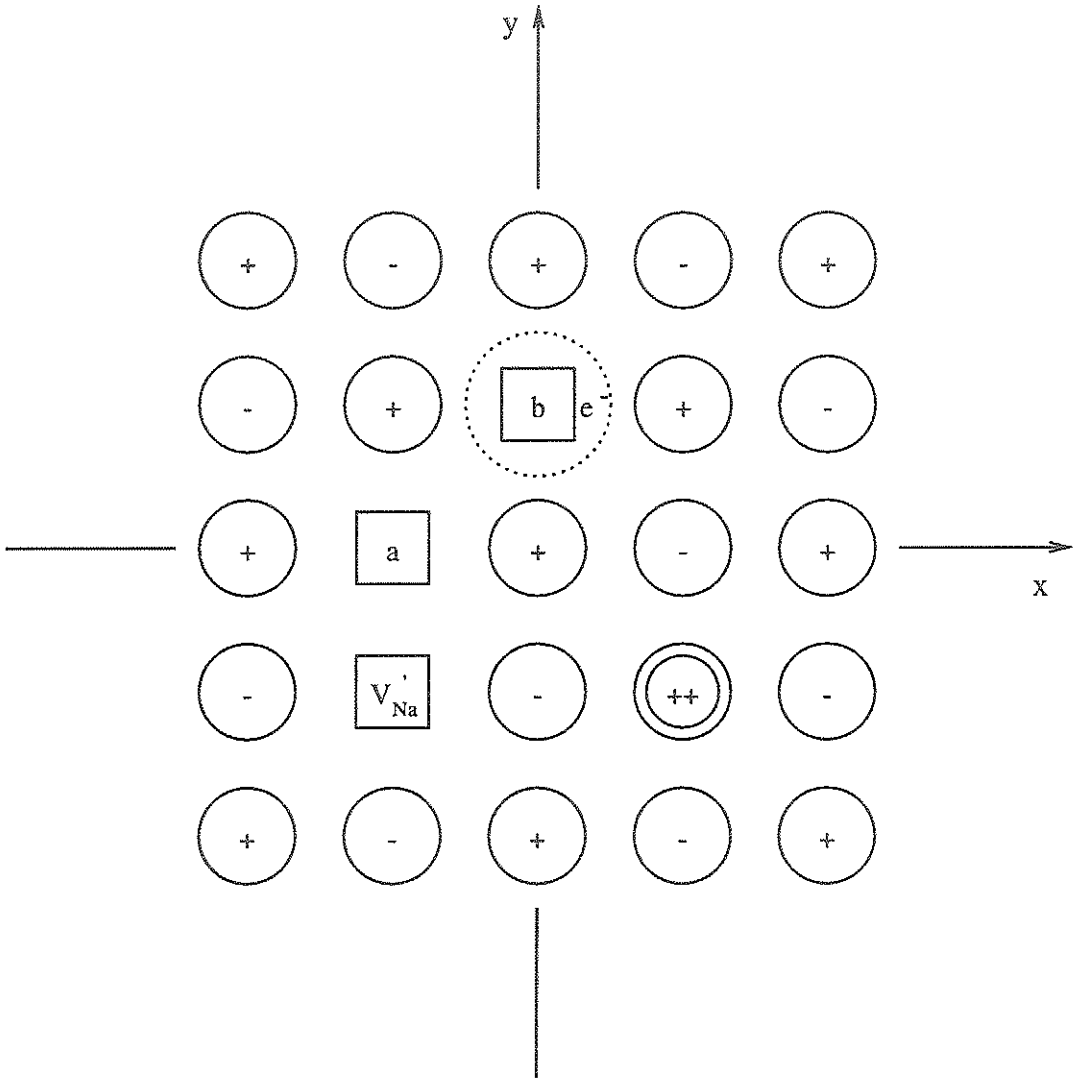

Figure 4.12: The $(F_2^+)^*$ center: configuration 8

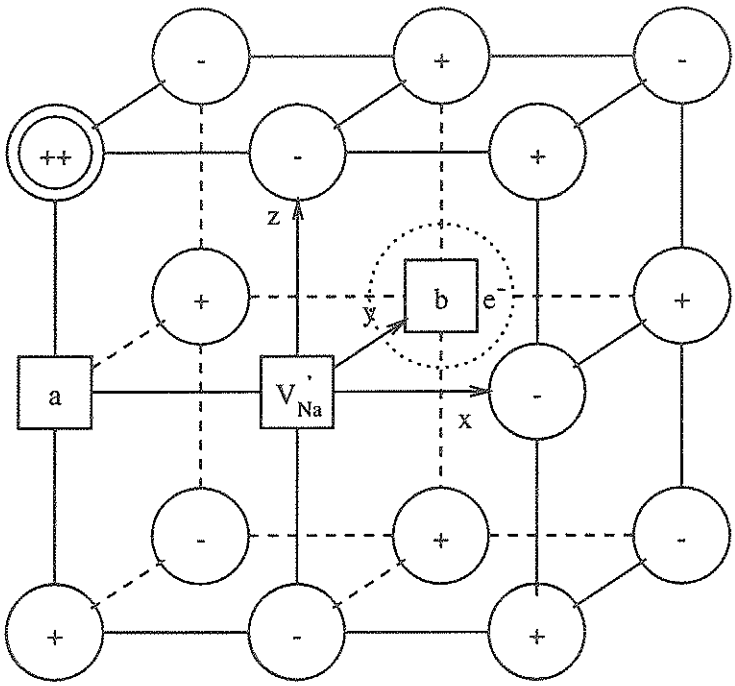

Figure 4.13: The $(F_2^+)^*$ center: configuration 9

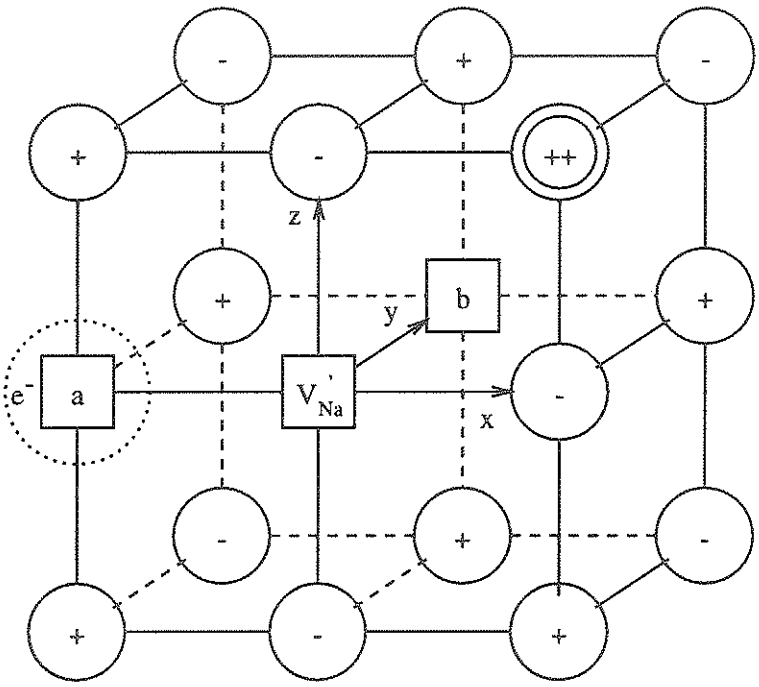

Figure 4.14: The $(F_2^+)^*$ center: configuration 10

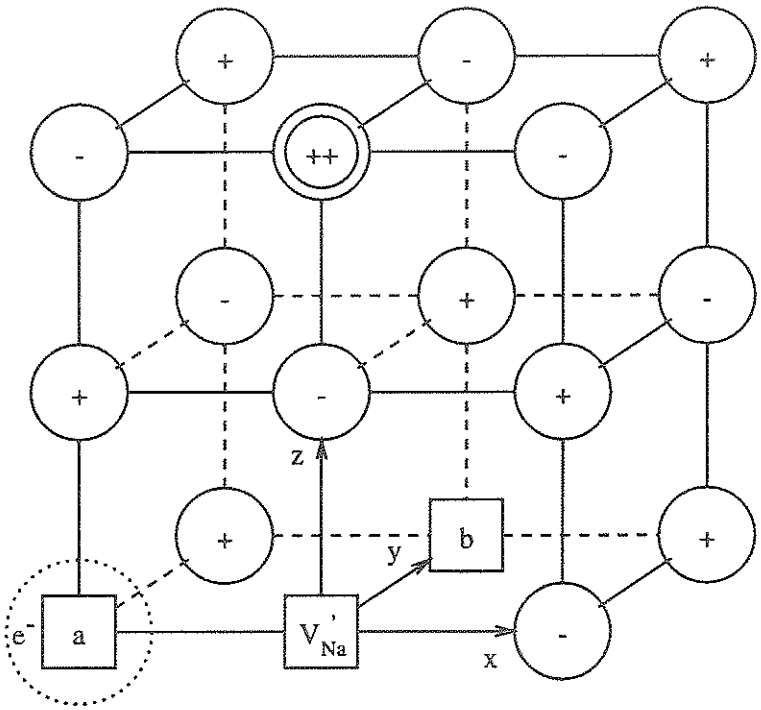

Figure 4.15: The $(F_2^+)^*$ center: configuration 11

Table 4.23: Results for the one-electron model of the $(F_2^+)^*$ center: 11 configurations. The V'_{Na} position $\mathbf{x}_{V'_{Na}}$ and Mg^{2+} position $\mathbf{x}_{Mg^{2+}}$ are in units of the perfect NaF lattice spacing a. E_I (eV) is the total ICECAP energy with unrelaxed positions of the F-center basis set centers. ΔE (eV) is energy lowering due to the relaxation of the basis set center distance, which is in units of a. P_M is the Mulliken population and Region I refers to a small region in which the HADES part of ICECAP relaxes the positions of all ions independently to minimize the total energy E_I.

			Region I(35 ions)			Region I(30 ions)			Relaxed Basis
No.	$\mathbf{x}_{V'_{Na}}$	$\mathbf{x}_{Mg^{2+}}$	E_I	ΔE	P_M	E_I	ΔE	P_M	Set Position
1a	0,0,0	0,$\overline{2}$,0	−14.96	0.03	1.0	−14.95		1.0	$\overline{1}$.05,0.00,0.00
1b	0,0,0	0,$\overline{2}$,0	−14.85		1.0	−14.85		1.0	
2	0,0,0	1,$\overline{1}$,0	−12.38	0.27	0.5	−10.98		0.5	$\overline{0}$.11,0.92,0.00
									$\overline{0}$.92,0.11,0.00
2a	0,0,0	1,$\overline{1}$,0	−14.89	0.03	1.0	−14.88		1.0	$\overline{1}$.05,0.00,0.00
3a	0,0,0	$\overline{1}$,$\overline{1}$,0	−12.17		1.0	−12.17		1.0	
3b	0,0,0	$\overline{1}$,$\overline{1}$,0	−13.81		1.0	−13.81		1.0	
4a	0,0,0	$\overline{2}$,0,0	–			–			
4b	0,0,0	$\overline{2}$,0,0	−13.47		1.0	−13.47		1.0	
5	0,0,0	$\overline{1}$,1,0	−7.63		0.5	−6.09		0.5	
5b	0,0,0	$\overline{1}$,1,0	−10.48		1.0	−10.48		1.0	
6a	$\overline{1}$,$\overline{1}$,0	0,$\overline{2}$,0	−14.25		1.0	−14.25		1.0	
6b	$\overline{1}$,$\overline{1}$,0	0,$\overline{2}$,0	−15.44	0.00	1.0	−15.44		1.0	0.00,1.01,0.00
7a	$\overline{1}$,$\overline{1}$,0	$\overline{2}$,$\overline{2}$,0	−14.07		1.0	−14.07		1.0	
7b	$\overline{1}$,$\overline{1}$,0	$\overline{2}$,$\overline{2}$,0	−14.79	0.00	1.0	−14.79		1.0	1.00,1.50,0.00
8a	$\overline{1}$,$\overline{1}$,0	1,$\overline{1}$,0	−14.03		1.0	−14.02		1.0	
8b	$\overline{1}$,$\overline{1}$,0	1,$\overline{1}$,0	−15.33	0.00	1.0	−15.33		1.0	0.01,1.00,0.00
9a	0,0,0	$\overline{1}$,0,1				–			
9b	0,0,0	$\overline{1}$,0,1				−13.46		1.0	
10a	0,0,0	1,0,1				−14.76	0.04	1.0	$\overline{1}$.05,0.00,0.00
10b	0,0,0	1,0,1				−14.55		1.0	
11	0,0,0	0,0,2				−12.19		0.5	
11a	0,0,0	0,0,2				−14.67	0.02	1.0	$\overline{1}$.05,0.00,0.00

important since they have higher total energies in any case. The last column gives the positions of the basis-set centers corresponding to the minimized total energy through cluster relaxation. In the table, the dash line '–' means there is no valid ICECAP (or HADES) calculation available.

From table 4.23, several important points can be seen immediately. First, if we sort these 11 configurations into two groups in terms of their Mg^{2+} impurity positions related to the anion-vacancy centers, the group with Mg^{2+} impurity at nearest-neighbor positions, including configuration 3, 4, 5 and 9, has higher energies than the other group, which contains configuration 1 (the Hofmann), 2, 6, 7, 8, 10 and 11. This is because the anion vacancies actually behave as positively charged objects due to the loss of negative charge, and therefore repel the net positively charged Mg^{2+} impurity. The second point concerns the electronic structure of atomistic configurations with the Na^{+} vacancy in an unsymmetrical position relative to the two anion vacancies. We put the excess electron at each anion vacancy center, a and b, alternatively. The electron prefers to localize at the center which is farther away from the negatively charged Na^{+} cation vacancy (configuration 6, 7 and 8). The third point is about symmetry breaking. It occurs in configurations 2, 5 and 11. We can see that for these configurations, when we break the symmetry by forcing the excess electron to localize at one of the anion vacancies, the total energies (unrelaxed) are lowered by 2.51 eV, 2.85 eV and 2.48 eV, respectively. This means that the symmetry-broken configurations are always preferred, producing single-vacancy localization for the excess electron. This agrees with the observation of Hofmann *et al.*

Table 4.23 also tells us that, for the group of configurations 1, 2, 6, 7, 8, 10 and 11, the difference of the relaxed total energy ($E_I - \Delta E$) between the two configurations with the highest energy (−14.69 eV in 11a) and the lowest energy (−15.44 eV in 6b) is 0.75 eV. Within such a small energy span, there are seven configurations, of

which the Hofmann model has the third lowest energy but it is only higher than the second by 0.37 eV and lower than the fourth by 0.07 eV. It would be quite difficult to compare them experimentally. Even for theoretical analysis and simulation, our methods cannot be assumed to be reliable to such a level of accuracy. In order to get a better understanding of the results we have obtained for these configurations, in table 4.24 we list seven of them with the low-lying relaxed total energies, and calculate their energy differences ΔE and accumulated energy differences relative to the lowest total energy (6b). We also calculate the corresponding temperatures in respect to these energies. From the table, it can be seen that although the energy differences are very small, the characteristic temperatures are spread out over a range of thousands Kelvin. This indicates that even though these configurations have very close total lattice energies, it is quite hard for them to convert thermally from one to another. Considering the room temperature approximately as 300 K, it corresponds to about 0.026 eV. We may not say that our simulation is accurate for the total energies within 0.03 eV. But we believe that it does give the correct trend, or ordering, about the energy differences for these configurations. We see that the narrowest energy difference, between 10a and 7b (0.007 eV), is still corresponding to a temperature slightly higher than liquid nitrogen temperature (77 K). The stablization energy between the lowest- and second lowest-energy configurations, namely 6b and 8b, is calculated to be 0.106 eV, which corresponds to a temperature of 1230 K. Thus at room temperature, $\sim$ 300 K, one would not expect significant conversion from 6b to 8b. We caution, however, that both of these configurations, having lower energies than the Hofmann model, are from a class of configurations that we have not fully investigated. These are the ones with the V'_{Na} at $(-1,-1,0)$, including case 7, which is of higher energy. It will be important to learn from future work whether there are still lower-energy configurations in this class, and also in the class with the V'_{Na} at $(-1,0,1)$. Furthermore, the characteristic temperature for conversion from

Table 4.24: The $(F_2^+)^*$-center ground state: configurations with low-lying energies. E_I (eV) is the total ICECAP energy with relaxation of the F-center basis set centers. ΔE, in units of eV, is the energy difference between one and the next, starting from lowest energy configuration 6b. $\sum \Delta E$ (eV) is the accumulated energy difference related to the 6b. The characteristic temperature T (K) corresponds to $\sum \Delta E$ and the Boltzmann's constant $k_B = 8.6171 \times 10^{-5}$ (eVK^{-1}).

No.	E_I (eV)	ΔE (eV)	$\sum \Delta E$ (eV)	$T = \sum \Delta E / k_B$ (K)
6b	−15.436	–	–	–
8b	−15.330	0.106	0.106	1230
1a	−14.987	0.352	0.449	5211
2a	−14.918	0.069	0.518	6011
10a	−14.798	0.120	0.638	7404
7b	−14.791	0.007	0.645	7485
11a	−14.693	0.098	0.743	8622

ground-state configuration to that of second-lowest energy will be of crucial interest. Also, to test the one-quantum-electron approach we have employed in the present simulation, we have to carry out several large quantum-cluster calculations and see whether they produce the similar ordering and energy differences. Certainly, investigating the physical nature of this center is not limited to the total lattice energy itself. A variety of research work has suggested that the cation impurity is playing an important role in improving the stability of the $(F_2^+)^*$-center laser action in alkali halide crystals.

Two principal conclusions follow from this work. One is that there appears to be configurations of lower energy than that of the Hofmann model for the $(F_2^+)^*$ center. The other is that, for all configurations studied so far, the excess electron, in the $(F_2^+)^*$ center in NaF:Mg in its ground state, localizes in a single anion vacancy, rather than in the characteristically symmetric two-vacancy configuration of the F_2^+ center. This result is in agreement with the experimental conclusion of Hofmann *et al.*

Chapter 5

Conclusions

Using many-electron unrestricted Hartree-Fock embedded quantum clusters, the ground states of the F and F_2^+ centers in NaF were studied; and the classical effective short-range potentials for the Mg^{2+}-F^- interaction, as well for the F-type center-ion interactions in NaF:Mg were derived. For the F-center ground state, we found that the center is, as expected, well localized in the center of the defect vacancy, and the displacements of its neighboring ions are negligible (section 4.3.1, tables 4.11). The charge transfer from the neighboring ions to the center is also very small, about (-0.01) electron charge (see table 4.12). In the case of the F_2^+ center, its ground state with the excess electron equally shared between two anion vacancies was examined (section 4.3.2). The distortion field is fairly large, with 10 nearest neighbors forced out by $5-7$ percent of the lattice spacing (table 4.13). The charge transfer from the neighboring ions into the center is (-0.09) electron charge, with (-0.95) charge in the s orbitals and (-0.14) charge in the overlapping p orbitals of the two vacancies (table 4.14). The Mg^{2+}-F^- short-range interaction (table 4.5), taken to be the Born-Mayer type, has a strong repulsive force but fairly short range. Table 4.17 shows that the short-range interactions between the F center and host ions can be fitted by the Buckingham potential, although they were found to be uncharacteristic of ions, with extremely strong attractive forces (large coefficients C). In contrast, the F center-Mg^{2+} interaction is found to have the Born-Mayer form with weak repulsive

force but very long range (ρ = 1.22 Å). The effective potentials between the F_2^+ center and host ions were also derived (section 4.4). Their behaviors are in good agreement with the results of many-electron quantum-cluster calculations.

The investigation of the atomistic and electronic structures of the $(F_2^+)^*$ center was carried out on the basis of the one-electron quantum-cluster model, using the effective short-range potentials (section 4.5). In all configurations, the F-center like single-vacancy localization was found for the $(F_2^+)^*$-center ground state. This agrees with the conclusion of Hofmann *et al.* Seven low-lying-energy configurations (figures 2.2, 4.6, 4.10, 4.11, 4.12, 4.14, 4.15) are listed in table 4.24 and are discussed in terms of characteristic temperature. Two configurations (6b and 8b) with lower-lying energies than that of Hofmann model were found. The stabilization energies seem to prevent conversion between different configurations at room temperature. This strongly indicates that there probably exist other configurations, which are more favorable as the atomistic model for the $(F_2^+)^*$ center than the Hofmann configuration, particularly since configurations 6b and 8b belong to a class which has not been completely investigated.

Finally, we conclude that the single-electron model for the $(F_2^+)^*$ center has successfully reduced the amount of work needed for investigating such a complicated center. Furthermore, the present work points to future investigation. First, using one-electron quantum-cluster simulation, other configurations should be studied to obtain all the low-energy configurations. Then for a restricted group, many-electron quantum-cluster simulation can be carried out to predict the stable configuration of the $(F_2^+)^*$ center.

Bibliography

[1] R.W. Pohl, Proc. Phys. Soc. London, **49**, extrapart 3 (1937)

[2] F. Seitz, Rev. Mod. Phys., **26**, 7 (1954)

[3] W.B. Fowler in *Physics of Color Centers*, W.B. Fowler ed., Academic Press, New York, 1968

[4] A.M. Stoneham, *Theory of Defects in Solids*, Clarendon Press, Oxford, 1975

[5] Y. Farge and M.P. Fontana, *Electronic and Vibrational Properties of Point Defects in Ionic Crystals*, North-Holland Publ. Company, Amsterdam, 1979

[6] G. Baldacchini, Cryst. Latt. Def. Amorph. Mater, **18**, 43 (1989)

[7] P. Avakian and A. Smakula, Phys. Rev., **120**, 2007 (1960)

[8] L.F. Mollenauer and S. Pan, Phys. Rev., **6**, 772 (1972)

[9] H.F. Ivey, Phys. Rev., **72**, 341 (1947)

[10] G. Baldacchini in *Advances in Nonradiative Processes in Solids*, preprint (1989)

[11] W. Hayes and A.M. Stoneham, *Defects and Defect Processes in Nonmetallic Solids*, Wiley Interscience Publ., New York, 1985

[12] F. Lüty in *Physics of Color Centers*, W.B. Fowler ed., Academic Press, New York, 1968

[13] L.F. Mollenauer, Opt. Lett., **1**, 164 (1977)

[14] L.F. Mollenauer and D.H. Olson, J. Appl. Phys.: D, **46**, 3109 (1979)

[15] D.H. Hofmann, F. Lohse, H.J. Paus, D.Y. Smith and J.-M. Spaeth, J. Phys. C: Solid State Phys., **18**, 443 (1985)

[16] L.F. Mollenauer, Opt. Lett., **5**, 188 (1980)

[17] H. Eisele, H.J. Paus and J. Wagner, IEEE J. Quant. Electron, **QE-18**, 152 (1982)

[18] A. Szabo and N.S. Ostlund, *Modern Quantum Chemistry*, McGraw-Hill, Inc., New York, 1989

[19] R.F. Marshall, R.J. Blint and A.B. Kunz, Phys. Rev. B, **13**, 3333 (1976)

[20] B.G. Dick and A.W. Overhauser, Phys. Rev., **112**, 90 (1958)

[21] A.B. Kunz and D.L. Klein, Phys. Rev. B, **17**, 4614 (1978)

[22] J.M. Vail, J. Phys. Chem. Solids, **51**, 589 (1990)

[23] C.R.A. Catlow, M. Dixon and W.C. Mackrodt, in *Computer Simulation of Solids*, C.R.A. Catlow and W.C. Mackrodt ed., chap. 1 and 10, Springer-Verlag, 1982

[24] J.M. Vail, A.H. Harker, J.H. Harding and P. Saul, J. Phys. C: Solid St. Phys., **17**, 3401 (1984)

[25] J.H. Harding, A.H. Harker, P.B. Keegstra, R. Pandey, J.M. Vail and C. Woodward, Physica **131B**, 151 (1985)

[26] M.J. Norgett, Atomic Energy Research Establishment Report, Harwell, No. R7650 (1974)

[27] J. Meng, R. Pandey, J.M. Vail and A.B. Kunz, Phys. Rev. B **38**, 10083 (1988) and references therein.

[28] R. Pandey and A.M. Stoneham, J. Phys. C **18**, 5289 (1985)

[29] R. Pandey and J.M. Vail, J. Phys: Condens. Matter **1**, 2801 (1989)

[30] C.R.A. Catlow, K.M. Diller and M.J. Norgett, J. Phys. C **10**, 1395 (1977)

[31] W.C. Mackrodt and R.F. Stewart, J. Phys. C **12**, 431 (1979)

[32] S. Huzinaga, *Gaussian Basis Sets for Molecular Calculations*, Elsevier, New York, 1984

[33] J. Meng, R. Pandey, J.M. Vail and A.B. Kunz, J. Phys.: Condens. Matter **1**, 6049 (1989)